Development of non-linear soil model for foundation reuse

by

Clara Seah (JE)

Fourth-year undergraduate project

in Group D, 2011/2012

I hereby declare that, except where specifically indicated, the work submitted herein is my own original work.

*Signed:*_________________________ *Date:*________________

Technical abstract for 4th year undergraduate project

Development of non-linear soil model for foundation reuse

By Clara Seah of Jesus College in Group D, 2011/2012

Foundation reuse has become increasingly popular recently, motivated by increasing ground congestion in highly urbanised cities like London. With increasing emphasis on sustainability in construction, pile reuse is a progressively more attractive option. However, reuse of piles is a fairly new concept in modern civil engineering and thus there remain key geotechnical concerns regarding pile behaviour during reuse, particularly in terms of the interaction between new and old piles. Thus, the main objective of this project is develop a new analysis tool for pile reuse projects for the existing Cambridge foundation software which has been developed by a former researcher, Leung Y.F., of the Cambridge University Engineering Department. The current software uses a finite element mesh to model foundation systems and analyses soil behaviour using elastic (Mindlin) and elastic-plastic load transfer approaches and does not fully consider the non-linear behaviour of soil at high strains. Thus, through this research, a novel analytical tool was developed in which soil behaviour was modelled using a non-linear load transfer approach by Kraft et al. The analytical tool is able to analyse foundation behaviour under cyclic loading (using an approach by Chin & Poulos) and is thus appropriate for the simulation of pile reuse behaviour. Furthermore, it is noted that curve-fitting modelling parameters in this tool can be adjusted to better fit field data to give a more accurate simulation. This novel analytical tool was validated against the existing elastic and elastic-plastic analysis methods and simulation results of all 3 numerical analysis methods were found to agree at low strains. At high strains, the new non-linear analysis method diverged from the existing 2 methods as soil non-linearity was accounted for in the new analytical tool. The new tool was further validated against field pile tests in London clay and of the 3 approaches, the new, non-linear load transfer approach was found to agree best with the field data, which also displayed soil non-linearity. Parametric tests were further conducted to show the effect of varying the curve-fitting modelling parameters and also to further validate that the tool was able to simulate soil behaviour under various foundation (e.g. raft thickness) and soil parameters (e.g. homogeneity of soil strength and stiffness). Finally, the new analytical tool was used to model the Bevis Marks foundation

reuse project in London clay, which was also instrumented with fibre optic cables to obtain strain data. A comparison of the numerical simulation to the field displacement data showed good agreement, with the numerical simulation giving a slightly conservative result. Simulations also showed that the differential deformations in the original and new Bevis Marks buildings were within safety limits to prevent building damage and it was further demonstrated that the presence of the raft increased the foundation stiffness and reduced differential deformations. It was also found that the Bevis Marks piles tended to carry a negative shaft resistance toward the pile head, indicating that movement of soft soil around the pile head was larger than the pile displacement. During unloading, pile deformation is elastically recovered due to relative low strains and high safety factors. In general, from this project, the new analytical tool developed has been shown to produce simulation results which agree with expected foundation behaviour. Future work can further validate this tool using more field data in various soil conditions and also gauge the performance of this software against other available software in terms of accuracy and speed. It is hoped that research on this analytical tool will continue and perhaps also incorporate thermal effects for the design of geothermal piles.

Table of Contents

List of Notations

α	Shaft adhesion factor
A_r	Area associated with raft node
A_p	Pile cross-sectional area
$\mathbf{B}$	Strain-displacement matrix
δ	Secant modulus degradation value
$\mathbf{D}$	Stress-strain matrix
E	Soil Young's Modulus
E_p	Pile Young's Modulus
E_r	Raft Young's Modulus
f_i	Input load at node i
$\mathbf{f}$	Vector of input loads
G	Soil shear modulus
G_i	Initial G
$\mathbf{k_e}$	Element stiffness matrix
$\mathbf{K_{total}}$	Stiffness matrix of overall system
$\mathbf{K_{soil}}$	Soil stiffness matrix
$\mathbf{K_{pr}}$	Stiffness matrix due to raft and pile stiffness
$\mathbf{K_{raft}}$	Raft stiffness matrix
$\mathbf{K_{struct}}$	Superstructure stiffness matrix
$\mathbf{K_{pile}}$	Pile stiffness matrix
$\mathbf{K_{1\text{-}pile}}$	Pile stiffness matrix for a single pile
$K_{soil,ij}$	Soil stiffness at node i due to force at node j (ith row, jth column of $\mathbf{K_{soil}}$)
$K^s_{soil,ii}$	Soil stiffness at shaft node i (ith row, ith column of $\mathbf{K_{soil}}$)
$K^b_{soil,ii}$	Soil stiffness at base node i (ith row, ith column of $\mathbf{K_{soil}}$)
$\boldsymbol{\lambda}_{\mathbf{soil}}$	Soil flexibility matrix = $\mathbf{K_{soil}}^{-1}$
$\lambda_{soil,ij}$	Displacements at point i due to a force at point j (ith row, jth column of $\boldsymbol{\lambda}_{\mathbf{soil}}$)
$\lambda^s_{soil,ii}$	Soil flexibility at shaft node i due to force at j (ith row, ith column of $\boldsymbol{\lambda}_{\mathbf{soil}}$)
$\lambda^b_{soil,ii}$	Soil flexibility at base node i due to force at j (ith row, ith column of $\boldsymbol{\lambda}_{\mathbf{soil}}$)
L_e	Pile element length
L	Pile length

ν	Soil Poisson's ratio
ν_r	Raft Poisson's ratio
n	Number of nodes in foundation system
N_c	Base adhesion factor
P	Vector of mobilised resistances at each node
$\mathbf{P_c}$	Vector of internal forces in foundation due to $\mathbf{K_{struct}}$, $\mathbf{K_{pr}}$
P_i	Mobilised pile-soil (or raft-soil) interface force at node i
$P_{f,i}$	Ultimate pile-soil (or raft-soil) interface force at node i
P_{fs}	Ultimate shaft-soil shear force
P_{fb}	Ultimate pile base-soil normal force
P_{fr}	Ultimate raft-soil normal force
P_s	Mobilised shear resistance at shaft
P_b	Mobilised base resistance on pile base
ρ	Non-homogeneity factor (ratio of G at pile mid-depth to G at base)
r	Radial distance from pile centre
r_o	Pile radius
r_m	Distance from pile centre where displacements are negligible
R_f	Hyperbolic curve-fitting constant
R_{fs}	R_f for shaft node
R_{fb}	R_f for base node
R_c	Curve-fitting constant for cyclic loading
R_u	R_c for unloading cycle
R_r	R_c for reloading cycle
s_u	Undrained shear strength
τ	Mobilised shear stress
τ_f	Shear stress at failure
τ_{rf}	Ultimate raft bearing stress
τ_{so}	Shear stress at pile soil interface
u_i	Displacement at node i
u	Vertical displacement vector

1.0 Introduction

Though the concept of foundation reuse has been around for many years – large structures like castles were often rebuilt on the foundations of their predecessors—it is only recently that foundation reuse has become increasingly popular in redevelopment projects largely due to ground congestion. However, there are many challenges due to the uncertainty of reusing foundations.

In this project, a novel tool was developed for the current foundation software to model foundation reuse behaviour and this was validated against current soil models and field data. Finally, the new tool was used to model the Bevis Marks foundation reuse project and results of the numerical simulation were compared to fibre optics strain data.

1.1 Scope of Study

In this research, the following was undertaken:

- A general understanding of foundation reuse and the Bevis Marks reuse project was conducted.
- A detailed understanding of the existing Cambridge foundation analysis software was conducted.
- A new analysis tool was developed for the software, which used a non-linear load transfer approach to model soil behavior.
- The new analysis tool was used to simulate the Bevis Marks foundations. Numerical simulation was then compared to actual field data to determine the accuracy of analysis.

1.2 Bevis Marks site overview

The Cambridge University Engineering Department (CUED) has a research interest in the Bevis Marks foundation reuse project in London, where 67 piles will be reused. Thus, a key objective of this research was to simulate the Bevis Marks foundations. During the course of this project, a site visit was made to Bevis Marks (which is still under construction). Fig 1.1 and 1.2 show the original building and current progress of the site. Fig 1.3 shows the original and new foundation layout for the original and new buildings. This sub-section provides some background information on Bevis Marks. Further details of the simulation will be discussed in section 6.

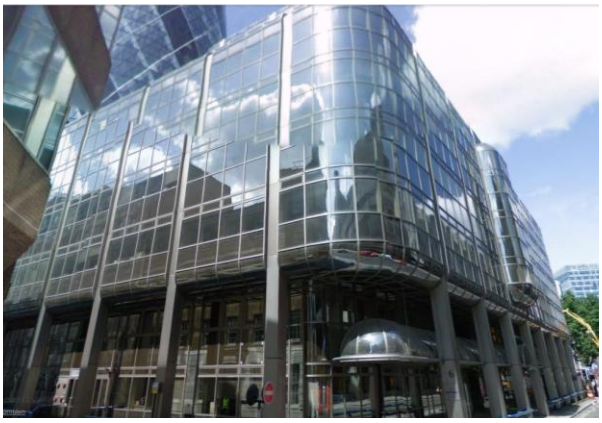

Fig 1.1: Original Bevis Marks building (Source: Google Maps) *Fig 1.2 Current Bevis Marks site (March 2012)*

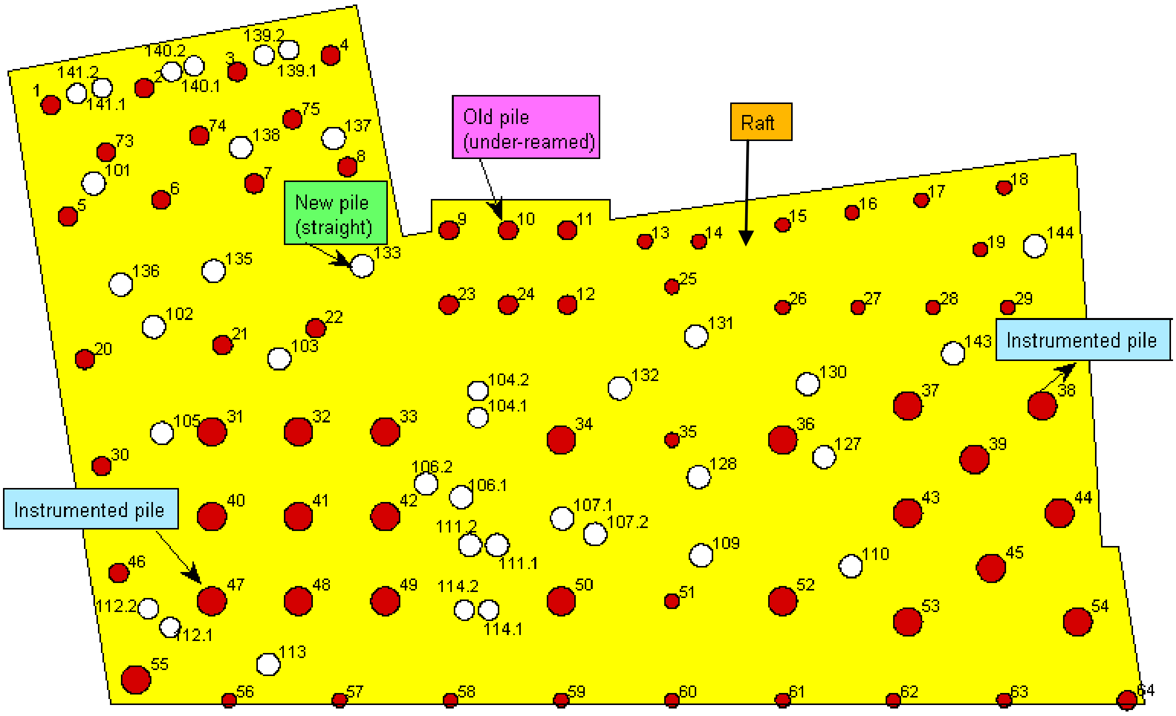

Fig 1.3: Foundation layout for old and new building at Bevis Marks

1.2.1 Ground conditions

Soil investigation data from Soil Consultants Ltd (SCL) has revealed that the Bevis Marks soil strata is relatively uniform throughout the site and is typical of London soil:

- 0-5m: Made ground at the surface
- 5-10m: terrace deposits
- 10-40m: London clay (variable depth of >30m) – all piles are located in this layer.
- >40m: Lambeth group

1.2.2 Original building

The original 1980s building was an 8-storey building with a double basement. Pile information was obtained from structural engineers Griffiths Cleator and Associates. The building was supported by 67 bored under-reamed piles attached to a basement slab (a raft). Building demolition was completed at the end of 2011.

1.2.3 New building

The new 16-storey building will have a single, double-height basement. Waterman proposed a foundation design which will reuse 67 existing piles alongside 37 new straight-shafted piles, as shown in Fig 1.3. A 1.0m transfer slab will be constructed on the existing basement slab to enable strain compatibility to be achieved between the new and existing piles. This effectively increases the raft thickness and is thought to help reduce differential deformations. Work on the new building began in 2012.

1.2.4 Fibre Optics Monitoring

CUED has instrumented 2 existing piles (piles 38 and 47 – see Fig 1.3) with optical fibre sensors for strain measurement. These were installed in September 2010 and strain measurements were obtained during the last 70% of the demolition process. Both strain and temperature cables were installed to account for temperature strain. Strain measurements will be compared to numerical simulation results of the Bevis Marks foundation.

2.0 Foundation Reuse

This section presents background research conducted on foundation reuse based largely on information from the Reuse of Foundation for Urban Sites (RuFUS) research project and focuses on the motivation, challenges and implementation process of reuse.

2.1 Motivation

- **Ground congestion**: This is a prime driver of reuse in cities where the working life of many buildings has greatly reduced. Repeated redevelopment has rendered the ground congested with piles which are expensive to remove thus increasing the attractiveness of reuse. In London, ground congestion has motivated reuse projects at Belgrave House (Vaziri & Windle (2006)) and Bevis Marks (Waterman (2010)).

- **Economic benefits:** Foundation reuse can generate cost savings for the project by cutting construction time (e.g. generates more rental income) and costs (e.g. material cost).
- **Sustainability**: Inherently, foundation reuse is a sustainable concept as it reduces the total embodied energy of a project and is thus increasingly used to reduce environmental impact.
- **Preservation of archaeology**: Foundation reuse can be an effective redevelopment solution to limit damage to a site's archaeological deposits. For instance, reusing foundations helped to limit damage to the ruins underlying the new Acropolis Museum in Athens (Stamatopoulos & Stamatopoulos (2006)).

2.2 Planning and implementation

According to RuFUS, the foundation reuse process should aim to assess and mitigate potential risks in foundation reuse. The process usually involves the following:

1. **Desk Study:** This involves finding records (drawings, calculations etc.) of existing foundations.
2. **Investigation of old piles**: This involves pile testing, determination of pile integrity etc.
3. **Evaluation of capacity** – focus of research. This involves determining if existing piles have sufficient capacity to carry new building loads. If not, additional piles may have to be constructed. It is noted that in design, reused and new piles are treated similarly. Typical pile design involves designing within ultimate limit states (ULS) due to foundation capacity and serviceability limit states (SLS) due to deformations. In deep foundations, differential deformations and relative deformations, which can lead to building damage, (see Appendix 1) usually govern design.
4. **Evaluation of alternatives**: This involves evaluating the feasibility and risk of various options e.g. whether to reuse piles, construct new piles etc.
5. **Monitoring during lifetime**: This includes the instrumentation of piles (both new and existing) to monitor pile performance.

2.3 Challenges

The performance uncertainty of reused foundations is a key concern. Reuse projects often present a set of unique challenges that conventional projects do not, such as:

- **Poor records**: Old records are required to determine existing pile information but may be difficult to trace. Without this information, reuse may be too risky to be viable.
- **Insufficient capacity**: Pile testing may reveal insufficient capacity for new loads. Thus, additional new piles may have to be installed.
- **Pile damage**: Pile testing is required to ensure pile integrity (e.g. no pile damage).
- **Incompatible column geometry**: Ideally, column and pile geometries should be closely linked – if the new column geometry for the new building differs greatly from existing pile geometry, foundation reuse may not be optimal. A raft can also be used to better distribute loads.
- **Owner/developer scepticism:** As foundation reuse may be perceived to be riskier than new foundations, project developers may prefer a conventional route instead.

With these challenges in mind, this project focuses on modelling reused pile behaviour to determine pile settlement so as to reduce uncertainty and risk, focusing particularly on the Bevis Marks project in London.

2.4 Research focus and reuse case studies

The main objective of this research was to develop a new tool for the Cambridge foundation software so as to better model foundation reuse behaviour (i.e. modelling of foundations under cyclic loading) to evaluate pile design for reuse projects. In particular, the main application of this research was to develop a tool to model the Bevis Marks reuse project. Thus, in order to better understand pile reuse behaviour, research on reuse case studies was conducted.

Konig et al. (2006) conducted pile tests on piles from a 42-year-old storehouse in Hamburg which were planned to be reused. The results from the 2005 pile tests were compared to old pile load test data from 1963 (when the piles were newly installed). The piles showed a significant increase in both stiffness and capacity over the 42 year period. Konig et al. postulated that this change in behaviour could be attributed to set-up as a result of consolidation, changes in the pile-soil friction coefficient, soil relaxation and small-amplitude cyclic loading.

Powell & Skinner (2006) presented the results of pile tests on ‘virgin’ and retested piles in London Clay over time. It was found that ‘virgin’ piles showed an increase in stiffness and capacity over the 4 years of study. However, it was found that retesting (for the first time) reduced pile capacity which then remained constant at this reduced level in subsequent retests. This is largely attributed to the strain softening behaviour of London Clay.

From the above, it is seen that reused pile response is not easily predicted and may depend on soil conditions. Thus, there is uncertainty in modelling pile reuse response and the interaction of reused piles with new piles. Hence, the current software was developed to allow the user to specify parameters to define the most likely response (Leung 2010) and subsequent development of the new analysis tool in this research also incorporated modelling parameters which can be adjusted to fit test data.

3.0 Literature review

As the main objective of this research project was to develop new analysis tools for the current Cambridge foundation software to better model reused piles, this chapter aims to review the approaches available in the current software. It also describes recent research on numerical modelling of non-linear soil behaviour over cyclic loading which has implications for modelling pile reuse.

3.1 Existing Cambridge Foundation Modelling Software

An initial understanding of the Cambridge foundation analysis tool was conducted to better understand the current software. The software was initially developed by Leung Y. F. in Mathematica and translated into C++ by Yan J. from the CUED. The current software models foundation systems (rafts and pile groups) using discrete elements and performs load-displacement simulations based on input loads as the boundary conditions in a numerical analysis.

The key input components of the software are:

- **Raft parameters:** geometry (raft thickness), material parameters (Young's Modulus, Poisson's ratio) and location
- **Pile parameters:** geometry (pile length and radius), material parameters (Young's Modulus, Poisson's ratio) and location
- **Soil parameters:** soil stiffness (E_{soil}), Poisson's ratio (ν) and undrained shear strength (s_u).
- **Superstructure stiffness:** obtained from superstructure FEM analysis
- **Force parameters:** Loading on foundation (from superstructure) including force magnitude and location
- **Mesh parameters:** Raft element length, pile element length.

The key output components are:

1) Finite Element Model (FEM) of the foundation
2) Numerical analysis of foundation (pile group with raft)

3.1.1 Finite Element Model (FEM) of the foundation

Using inputs above, the software discretises the foundation into finite elements and nodes. The raft is modelled as a thin plate discretised into 3-node, 2-dimensional triangular elements with 3 degrees of freedom (d.o.f.) (vertical displacement and rotation in 2 directions) so that the bending stiffness of the raft is modelled. The pile is discretised into 1-dimensional bar elements with 1 d.o.f. (vertical displacement) with the pile and raft sharing nodes at the pile head. Fig 2 shows a representation of the discretised foundations.

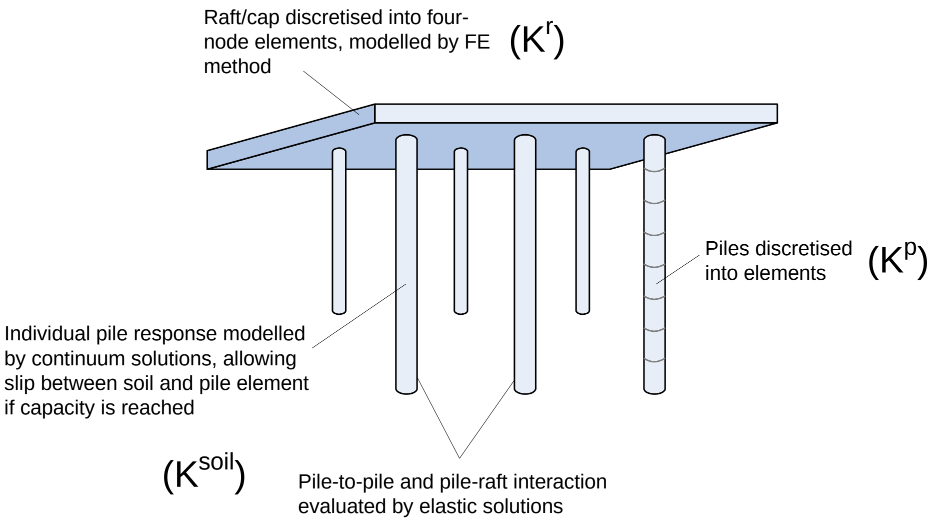

Fig 2: Schematic representation of pile-raft discretised model (Leung (2010))

The discretisation process results in 4 types of nodes:

- Raft nodes: nodes which are only on the raft
- Raft/pile-head nodes: nodes shared by both the raft and the pile (must be pile head)
- Regular pile nodes (includes pile head nodes not on raft): nodes on pile (models shaft capacity)
- Pile end nodes: models base capacity

3.1.2 Pile group/pile-raft analysis

The software numerically analyses pile displacement behaviour using soil, superstructure, pile and raft parameters to yield an overall stiffness to solve the following system of equations as given in [1] where an overall stiffness matrix, $\mathbf{K_{total}}$, is used to describe the interactions between nodes due to the stiffness of the soil, raft, pile and superstructure. Given $\mathbf{K_{total}}$ and the force vector, **f**, [1] can be used to solve for the displacement vector **u**.

$$\mathbf{K_{total}u} = \left(\mathbf{K_{soil}} + \mathbf{K_{pile}} + \mathbf{K_{raft}} + \mathbf{K_{struct}}\right)\mathbf{u} = \left(\mathbf{K_{soil}} + \mathbf{K_{pr}} + \mathbf{K_{struct}}\right)\mathbf{u} = \mathbf{f} \text{ --- [1]}$$

$$\text{where } \mathbf{K_{total}} = \mathbf{K_{soil}} + \mathbf{K_{pile}} + \mathbf{K_{raft}} + \mathbf{K_{struct}}$$

$$\mathbf{K_{pr}} = \mathbf{K_{pile}} + \mathbf{K_{raft}}$$

Elaboration of how $\mathbf{K_{soil}}$, $\mathbf{K_{pile}}$, $\mathbf{K_{raft}}$ and $\mathbf{K_{struct}}$ are computed is given in the following sections. It is noted that the inverse of the stiffness matrix, **K**, is the flexibility matrix, λ.

*3.1.2.1 Formulation of soil stiffness matrix (**K_{soil}**)*

Soil is inherently a non-linear, non-homogenous medium, which makes it difficult to model and often requires greater computational effort. However, several researchers, including Chow (1986), have stated that nonlinear behaviour generally occurs at large strains near the vicinity of the piles while further away, soil behaviour is approximately elastic. Thus, in the software, pile-soil-raft and pile-soil-pile interaction is modelled using the elastic (Mindlin) solution. Individual pile response has been simulated either using the elastic solution or using elastic-plastic load transfer approach by Klar et al (2007).

1) **Elastic (Mindlin) solution**

Mindlin (1936) presented elastic solutions for the relationships between a point load (P) and the corresponding displacements (u) in a homogenous, isotropic elastic half-space (Fig 3). This method assumes soil linearity which does not capture non-linear soil response. However, since non-linearity is confined to a narrow zone of soil around the pile shaft (Chow 1986), pile-soil-raft interaction is generally thought to be well approximated using Mindlin's solution.

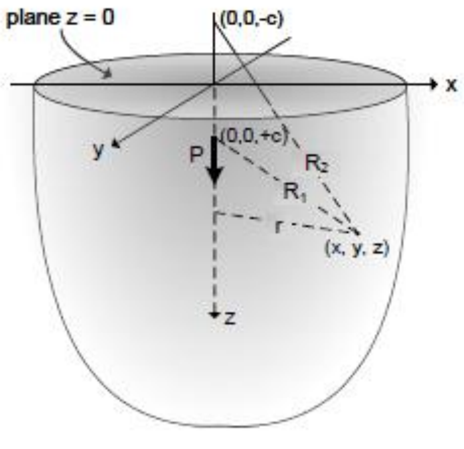

Figure 3: Illustration of Mindlin's solution (Leung (2010))

The Mindlin solution for the displacement u at a point (x, y, z) due to a point load P acting in a homogenous isotropic semi-infinite solid is given in [2].

$$u = \frac{P}{16\pi G(1-\nu)}\left[\frac{3-4\nu}{R_1} + \frac{8(1-\nu)^2-(3-4\nu)}{R_2} + \frac{(3-4\nu)(z+c)^2-2cz}{{R_2}^3} + \frac{(z-c)^2}{{R_1}^3} + \frac{6cz(z+c)^2}{{R_2}^5}\right] \text{------- [2]}$$

where c, z, R_1 and R_2 are defined in Fig 3.

Eqn [2] is the basis for determining $\lambda_{soil,ij}$ in $\boldsymbol{\lambda}_{\mathbf{soil}}$ i.e. the elastic displacements at point i due to a force at point j. However, $\lambda_{soil,ii}$ cannot be determined in the same way as there exists a singularity at the point of loading (i=j, R_1=R_2=0) thus, $\lambda_{soil,ii}$ is evaluated by determining the displacement at a node due to uniform load around the pile shaft (for pile node) or, for pile base and raft nodes, $\lambda_{soil,ii}$ is evaluated by integrating the elastic solutions over the associated areas (Leung 2010). $\mathbf{K}_{\mathbf{soil}}$ is obtained by then inverting $\boldsymbol{\lambda}_{\mathbf{soil}}$.

2) **Elastic-plastic load transfer solution (**Klar et al 2007)

The software uses an iterative bilinear solution to approximate non-linear soil behaviour. Effectively, a slip element is incorporated into the continuum solution to limit the contact stresses between the soil and the foundations (see [3]). Once the limiting stress is reached, slippage occurs at the node, and further increases in load will be redistributed to other nodes. Fig 4 shows a schematic representation of the elastic-plastic load-transfer method.

$$\mathrm{P_i} = \langle \mathbf{f} - (\mathrm{K_{pile}}+\mathrm{K_{raft}}+\mathrm{K_{struct}})\mathbf{u}\rangle_\mathrm{i} = \min[\langle \mathbf{f} - (\mathrm{K_{pile}}+\mathrm{K_{raft}}+\mathrm{K_{struct}})\mathbf{u}\rangle_\mathrm{i}, \mathrm{P_{f,i}}] \text{ ---- [3]}$$

where P_i = force on pile-soil interface at node i

$P_{f,i}$ = maximum contact stress at node i

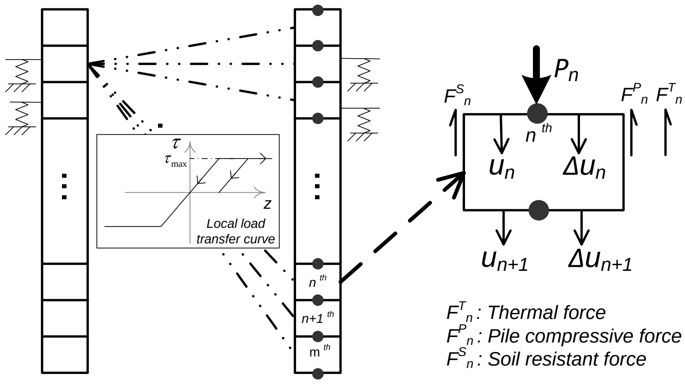

Fig 4: Schematic representation of elastic-plastic load transfer method (Leung (2010))

For pile node along the pile shaft or at the pile head, P_f refers to pile shaft capacity, P_{fs}, which is governed by [4] using the α-method for clayey soils (undrained failure).

$$\mathrm{P_{fs}} = \mathrm{s_u} \times \text{Surface area of shaft element} = 2\pi \mathrm{r_o L_e} \alpha \mathrm{s_u} \text{ ----------- [4]}$$

For London clay, α = 0.4-0.6 is generally accepted, based on empirical studies.

For a node at the base of the pile, f_{lim} refers to the base capacity of the pile, P_{fb} given in [5].

$$\mathrm{P_{fb}} = \mathrm{N_c s_u} \times \text{Base area} = \mathrm{N_c} \pi \mathrm{r_o}^2 \mathrm{s_u} \text{ ----------- [5]}$$

where usually $N_c = 9$ (Skempton, 1951)

For nodes on the raft, f_{lim} refers to the ultimate bearing capacity P_{fr} given in [6].

$$P_{fr} = A_r \tau_{rf} \text{ ----------- [6]}$$

$$\tau_{rf} \approx 1000\text{kPa for London Clay}$$

*3.1.2.2 Formulation of raft and pile stiffness matrices (**K_{raft}** and **K_{pile}**)*

$\mathbf{K_{raft}}$ and $\mathbf{K_{pile}}$ are formed using the element stiffness matrix, $\mathbf{k_e}$ in equation [7]. Element stiffness matrices of each element are then assembled to obtain global stiffness matrices, $\mathbf{K_{raft}}$ and $\mathbf{K_{pile}}$.

$$\mathbf{k_e} = \int_{V_e} \mathbf{B^T D B} dV \text{ ------- [7]}$$

For 1D pile elements,

$$D = E_p A_p \text{ -------- [8]}$$

Using a linear, 2 –node bar element, $\mathbf{k_e} = \frac{E_p A}{L_e}\begin{bmatrix} 1 & -1 \\ -1 & 1 \end{bmatrix}$ -------- [9]

Hence from [9], for one pile, $\mathbf{K_{1-pile}} = \frac{E_p A}{L_e}\begin{bmatrix} 1 & -1 & 0 & \dots & 0 \\ -1 & 2 & -1 & \dots & 0 \\ 0 & -1 & 2 & \dots & 0 \\ \vdots & \vdots & \vdots & \ddots & -1 \\ 0 & 0 & 0 & -1 & 1 \end{bmatrix}$ ----- [10]

$\mathbf{K_{1\text{-}pile}}$ for each pile can be assembled to form $\mathbf{K_{pile}}$.

For triangular raft elements in 2D with 3 degrees of freedom, assuming plane stress, from Leung (2010), the following values of **D** is used to construct $\mathbf{K_{raft}}$.

$$\mathbf{D} = \frac{E_r}{1-\nu_r^2}\begin{bmatrix} 1 & \nu_r & 0 \\ \nu_r & 1 & 0 \\ 0 & 0 & \frac{1-\nu_r}{2} \end{bmatrix} \text{ ---------------- [11]}$$

B is the strain displacement matrix from Zienkiewicz & Taylor (2005).

*3.1.2.3 Formulation of superstructure stiffness (**K_{struct}**)*

Leung (2010) incorporated superstructure effects on the stiffness of the foundation system through the superstructure stiffness matrix, $\mathbf{K_{struct}}$. $\mathbf{K_{struct}}$ is generated by applying a unit displacement at each column and calculating the reaction forces at all other supports, as shown in Fig 5, where a unit displacement at node 1 results in reaction forces R_j at other nodes such that $K_{struct,j1}=R_j$.

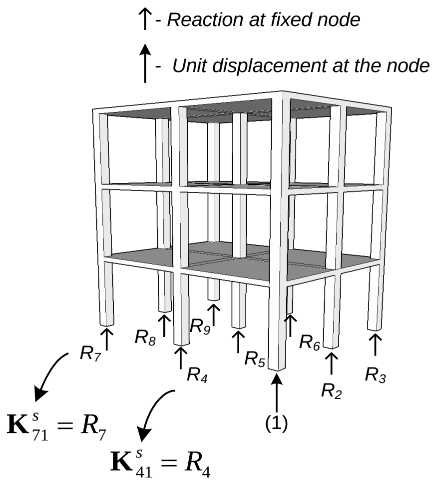

*Fig 5: Formulation of **K_{struct}** (Leung(2010))*

3.1.3 Limitations of existing software

With respects to modelling foundation reuse behaviour, the current Cambridge foundation modelling software does not model non-linear soil behaviour well as it only uses a elastic-plastic bilinear method. In addition, the current software is not able to model piles under cyclic loading in foundation reuse. Thus, the following sections describe recent research which would enable the above limitations to be overcome.

3.2 Non-linear load transfer soil models

In this section, a literature review is presented to find new techniques for modelling of soil non-linearity. The literature review reveals interesting techniques to model the non-linear behaviour of piles as part of a pile group and cyclically.

The load transfer method is commonly used to predict the load-displacement behaviour of piles using discrete pile elements. The approach utilises load transfer t-z curves to represent the relationship between mobilised shaft friction ('t') and pile movement relative to the soil (‘z’) which are used to simulate the pile-soil interaction along the depth of the pile. Fig 6 gives an illustration of the load transfer method, showing that soil non-linearity is incorporated using a non-linear load transfer relationship. In this section, the basis of the load transfer approach will be discussed based on a single pile and modifications required for pile group and cyclic loading analysis will be further discussed.

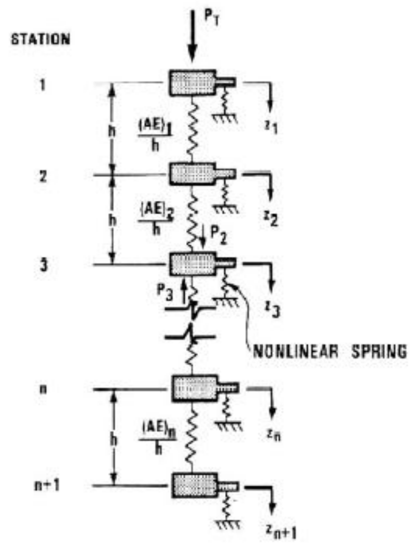

Fig 6: Idealisation of load transfer method (Leung (2010))

3.2.1 Non-linear load transfer approach for a single pile

From Fig 6, it can be seen that, the load transfer approach uses a non-linear spring to represent the interaction between each shaft node and the soil. The base response is associated with the spring at the pile end node. The load transfer approach assumes no interaction between nodes of the same pile i.e. that the non-linear spring response is independent of one another. Thus, in formulating the soil stiffness matrix (e.g. $\mathbf{K_{soil}}$) for a single pile, the off-diagonal components of the matrix will be zero (Chow 1986) (see [15]). Thus, the load transfer approach does not model the soil continuum rigorously but Leung (2010) asserts that the load transfer method enables the non-linearity of soil behaviour to be modelled easily, making it a popular approach favoured by many researchers.

According to Chow (1986), there exist many empirically-determined load-transfer curves used, particularly in the offshore industry. However, Kraft et al. (1981) proposed a rational t-z relationship based on the theoretical work of Randolph & Worth (1978). It is based on this approach that Chow (1986) and Chin & Poulos (1991) developed their pile group and cyclic loading load transfer approaches that will be discussed in later sections. Thus, the methodology presented in this paper will be based on the work of Kraft et al. which is described briefly here.

The load-displacement relationship given by Randolph & Worth's continuum solution is:

$$\text{Vertical displacement, } u = \tau_{so} r_o \int_{r_o}^{r_m} \frac{dr}{Gr} \text{ ------- [12]}$$

From Kraft et al., for constant G (linear soil), the soil stiffness at node i due to a force at node i is given by:

$$\text{Soil stiffness on pile shaft, } K^{s}_{soil,ii} = \frac{2\pi G L_e}{\ln(r_m/r_o)} \text{ ------- [13]}$$

$$\text{Soil stiffness at pile base, } K^{b}_{soil,ii} = \frac{4 G r_o}{1-v} \text{ ------- [14]}$$

As there is no interaction between nodes of the same pile, there is no stiffness coefficient associated with these springs (see [15]).

$$K_{soil,ij} = 0 \text{ where i, j are nodes on the same pile and i≠j ----- [15]}$$

As soil is inherently non-linear, a hyperbolic shear-stress—shear-strain relationship has been suggested by Kraft et al. to approximate the non-linear behaviour of soil:

$$\text{tangent shear modulus, } G = G_i \left(1 - \frac{\tau R_f}{\tau_f}\right) \text{---------- [16]}$$

Hence, the tangent soil stiffness is given by:

$$K^{s}_{soil,ii} = \frac{2\pi G L_e}{\ln\left(\frac{r_m - \beta_s}{r_o - \beta_s}\right) + \frac{\beta_s (r_m - r_o)}{(r_m - \beta_s)(r_o - \beta_s)}} \text{ ------- [17]}$$

$$K^{b}_{soil,ii} = \frac{4 G r_o}{1-v} (1 - \beta_b)^2 \text{ ------- [18]}$$

$$\beta_s = \frac{P_s r_o R_{fs}}{P_{fs}} \text{ --------- [19]}$$

$$\beta_b = \frac{P_b r_o R_{fb}}{P_{fb}} \text{ --------- [20]}$$

where R_{fs}, R_{fb}= hyperbolic curve fitting constants for shaft and base respectively

According to Chin & Poulos, limited experience suggests that R_{fs}=0-0.5 and R_{fb}≈0.9.

3.2.2 Load transfer approach for cyclic axial loading of piles

A simple and efficient cyclic loading approach was developed by Chin & Poulos. It utilises Masing's criteria to describe the unload-reload stress-strain response of the springs at the pile-soil interface as shown in Fig 6. Fig 7 shows Chin & Poulos' cyclic hyperbolic stress-strain soil model. The initial “backbone” curve (curve 1 in Fig 6) is given by the hyperbolic equation in [21] using [13] to [20].

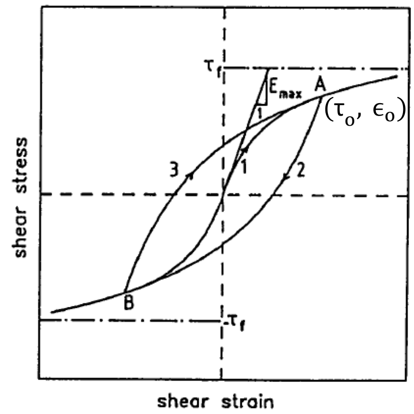

Fig 7: Non-linear shear-stress—shear-strain relationship (Chin & Poulos (1991))

$$\tau = \frac{E_{max}\epsilon}{[1+(R_f E_{max})|\epsilon/\tau_f|]} \text{ ---------- [21]}$$

where E_{max} = initial tangent modulus at small strains (Fig 7)

ϵ = current shear strain

Masing’s criteria is described here:

1) The initial slope of the unloading and reloading curves (curves 2 and 3 in Fig 7 respectively) will be equal to E_{max}.
2) The shape of the unloading and reloading curves will be similar to the “backbone” but scaled by a factor of 2.

Using a modified form of the Masing’s criteria, Poulos and Chin propose the unloading and reloading curves shown in Eqn. [22] and [23] respectively.

$$\tau - \tau_o = \frac{E_{max}(\epsilon-\epsilon_o)}{[1+(R_f E_{max}/2R_u)|(\epsilon-\epsilon_o)/\tau_f|]} \text{ ---------- [22]}$$

$$\tau - \tau_o = \frac{E_{max}(\epsilon-\epsilon_o)}{[1+(R_f E_{max}/2R_r\delta)|(\epsilon-\epsilon_o)/\tau_f|]} \text{ ---------- [23]}$$

where (τ_o, ϵ_o) is the point of load reversal (A and B on Fig 7)

R_u, R_r = curve-fitting constants for unloading and reloading curves respectively

δ =Secant modulus degradation value

It is noted that R_u and R_r can be adjusted to match available test data. For the present work, it is assumed that $R_u = R_r = \delta = 1.0$.

Thus, for cyclic loading, the unloading and reloading curves can be modelled using equations [13]-[18] using adjusted values of β_s and β_b as given in equations [24] and [25].

$$\beta_s = \frac{|P_s - P_{so}| r_o R_{fs}}{2R_c \delta |P_{fs}|} \text{ --------- [24]}$$

$$\beta_b = \frac{|P_b - P_{bo}| r_o R_{fb}}{2R_c \delta |P_{fb}|} \text{ --------- [25]}$$

where $R_c = R_u$ or R_r (unloading or reloading)

P_{so}, P_{bo} = mobilized pile shaft, base resistance at load reversal

Poulos and Chin's numerical approach shows good agreement with field results of a pile load tested under cyclic loading.

3.2.3 Load transfer approach for pile groups

Chow (1986) presented a simple, hybrid approach to analyse the behaviour of pile groups using the load transfer method. Essentially, in a pile group, the overall settlement of a pile is due to its own loading plus the effect of loads on other piles. Discretising the foundation system into n nodes (e.g. in a finite element system), this effect can be expressed as follows:

$$\text{Displacement at node i, } u_i = \sum_{j=1}^{n} \lambda_{soil,ij} f_j \text{ ----------- [26]}$$

Applying [26] to each node, the matrix equation [27] can be obtained:

$$\mathbf{u} = \boldsymbol{\lambda}_{\mathbf{soil}} \mathbf{f} \text{ ----------- [27]}$$

where $\boldsymbol{\lambda}_{\mathbf{soil}}$ = soil flexibility matrix = $\mathbf{K}_{\mathbf{soil}}{}^{\mathbf{-1}}$

$\lambda_{soil,ii}$ for nodes on the pile shaft and base are reciprocals of equations [13]-[18] and are given in equations [28]-[31].

For linear soil behaviour,

$$\text{Flexibility coefficient on shaft, } \lambda^{s}_{soil,ii} = \frac{\ln(r_m/r_o)}{2\pi G L_e} \text{ ------- [28]}$$

$$\text{Flexibility coefficient on base, } \lambda^{b}_{soil,ii} = \frac{1-\nu}{4Gr_o} \text{ ------- [29]}$$

For non-linear soil behaviour,

$$\text{Flexibility coefficient on pile shaft, } \lambda^{s}_{soil,ii} = \frac{\ln\left(\frac{r_m - \beta_s}{r_o - \beta_s}\right) + \frac{\beta_s (r_m - r_o)}{(r_m - \beta_s)(r_o - \beta_s)}}{2\pi G L} \text{ ------- [30]}$$

$$\text{Flexibility coefficient on pile base, } \lambda^{b}_{soil,ii} = \frac{1-\nu}{4Gr_o(1-\beta_b)^2)} \text{ ------- [31]}$$

where β_b and β_s are defined in [19] and [20]

For interactions between piles in a pile group, Chow (1986) proposes a hybrid model where interactions between nodes not of the same pile are modelled elastically using the Mindlin solution in equation [2]. This results in a flexibility coefficient shown in [32] as non-linear behaviour is generally confined to a narrow zone around each pile such pile-soil-pile and pile-soil-raft interactions are largely linear-elastic.

$$\lambda_{\mathrm{soil,ij}} = \frac{1}{16\pi G(1-\nu)}\left[\frac{3-4\nu}{R_1} + \frac{8(1-\nu)^2-(3-4\nu)}{R_2} + \frac{(3-4\nu)(z+c)^2-2cz}{{R_2}^3} + \frac{(z-c)^2}{{R_1}^3} + \frac{6cz(z+c)^2}{{R_2}^5}\right] \text{------- [32]}$$

where i≠j and i, j are nodes that are not on the same pile

and c, z, R_1 and R_2 are defined in Fig 3

From [15],

$$\lambda_{\mathrm{soil,ij}} = 0 \text{ for i≠j and i, j are nodes on the same pile ------- [33]}$$

The use of Mindlin's solution to determine interaction effects is only approximate, especially for non-linear soil behavior (Chow (1986)). This is because, before full slippage at a particular node has taken place, the non-linear soil behaviour adjacent to the pile shaft introduces a discontinuity in the material property.

Thus, Chow (1986) proposes that, for a node i where shear strength is fully mobilised, i.e. mobilised resistance P_i=limiting resistance $P_{f,i}$, equation [34] applies.

$$\lambda_{\mathrm{soil,ji}} = \lambda_{\mathrm{soil,ij}} = 0 \quad \forall\, j \in \mathbb{Z},\ 1 \le j \le n \text{ ------- [34]}$$

where n=total number of nodes

Applying [28]-[33] give $\boldsymbol{\lambda}_{\mathbf{soil}}$ which can be inverted to give $\mathbf{K}_{\mathbf{soil}}$. $\mathbf{K}_{\mathbf{soil}}$ can be assembled into equation [1] to yield $\mathbf{K}_{\mathbf{total}}$ which can be inverted to obtain the displacement solution.

Comparison of numerical analysis of pile group behaviour using Chow's hybrid method gives good agreement with field tests on pile groups in overconsolidated soils, including London Clay (Chow 1986), using R_f=0.9.

4.0 Development of new analysis tool (non-linear cyclic load transfer soil model)

From section 3.1, the current foundation analysis tool does not model the non-linearity of soil behaviour well and does not have the capabilities to model foundation systems under cyclic loading during reuse. Section 3.2 revealed interesting techniques to model pile groups in non-linear soil undergoing cyclic loading. Thus, it is the focus of this research to develop a novel and more accurate non-linear cyclic soil model for pile groups.

This section will focus on the development of a new, non-linear cyclic load transfer solver based on the cyclic loading approach by Chin & Poulos (1991) and the pile group analysis approach formulated by Chow (1986) to modify the load transfer approach by Kraft et al (1981). This numerical code will be parametrically tested in following sections and will be compared against the elastic and elastic-plastic solutions in the current software and validated against field tests.

4.1 Implementation procedure

As this approach uses a non-linear, cyclic load transfer solution for pile groups given by Chin & Poulos (1991) and Chow (1986), the soil stiffness matrix, $\mathbf{K_{soil}}$, is formulated by first calculating the flexibility matrix $\boldsymbol{\lambda_{soil}}$ using the following principles:

- The flexibility coefficient, $\lambda_{soil,ii}$, for node i on pile nodes (either shaft or base) can be calculated using the load transfer approach by Kraft et al. from equations [28]-[29] (initially) and [30]-[31]. During initial loading (e.g. monotonic backbone curve in Fig 7) β_s and β_b are given by [19] and [20] respectively. During cyclic loading (unloading or reloading), β_s and β_b are given by [24] and [25] respectively, assuming $R_c = \delta = 1.0$.
- As the load transfer approach assumes no interaction between nodes of the same pile, $\lambda_{soil,\ ij} = 0$ for $i \neq j$ where i and j are nodes of the same pile from equation [33].
- From Chow (1986), it is assumed that the raft-soil-raft, pile-soil-pile and pile-soil-raft interaction is approximately elastic. Thus, the flexibility coefficient, $\lambda_{soil,ij}$, for nodes not on the same pile is given by the Mindlin solution in [32].
- $\boldsymbol{\lambda_{soil}}$ is then inverted to obtain $\mathbf{K_{soil}}$.

Having obtained $\mathbf{K_{soil}}$, with $\mathbf{K_{pile}}$, $\mathbf{K_{raft}}$ and $\mathbf{K_{struct}}$ formulated the same way as in section 3.1, the following is used to obtain the load-displacement relationship of the foundations.

From [1],

$$\mathbf{u} = \mathbf{K_{total}}^{-1}\mathbf{f} \text{ -------------- } [35]$$

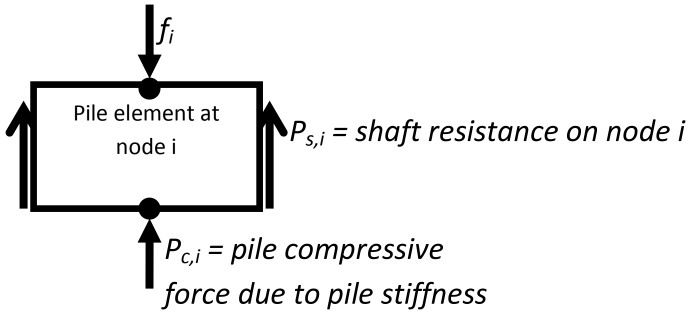

Fig 8: Schematic representation of forces on a pile shaft element

Fig 8 gives a schematic representation of forces on a pile shaft element which shows that external forces are transmitted through the foundation system via internal forces, $\mathbf{P_c}$, in [36].

$$\mathbf{P_c} = (\mathbf{K_{pr}} + \mathbf{K_{struct}})\mathbf{u} \text{ ----------- } [36]$$

Thus, mobilised forces on foundation-soil boundaries (e.g. shear forces on pile shaft, reaction forces under pile base and raft) are given by vector **P** in [37].

$$\mathbf{P} = \mathbf{f} - \mathbf{P_c},\ \mathrm{P_i} \leq \mathrm{P_{f,i}} \text{--------- } [37]$$

Where $P_i = P_s$, P_b or P_r depending on node i

$P_{f,i}$ = limiting contact forces (P_{fs}, P_{fr}, P_{fb} from Eqns [4]-[6]) at node i

From Chow (1986), once full slippage takes place at a node, there will be no interaction through the soil between that node and the remaining nodes in the pile group. Thus, once the shear strength of the soil is fully mobilised at a particular node, equation [34] applies and additional loads are transferred to neighbouring elements.

The above procedure is implemented iteratively and incrementally. Further details of the iterative procedure are given in Appendix 2.

The new tool allows foundation parameters to be altered between cycles. For instance, in reusing foundations, new piles are often used in addition to reused piles while raft thickness may change to accommodate higher loads. Thus, the non-linear cyclic load transfer software has been adapted to allow key parameters to be altered between cycles to better simulate foundation reuse. This is shown in the Bevis Marks simulation in section 6.

Given that pile reuse response is uncertain (see section 2.4), the analysis tool gives scope for the refinement of simulation results through modelling parameters R_{fs} and R_{fb} (hyperbolic curve fitting constants), which can be adjusted to better fit field data. Recommended values of R_{fs} and R_{fb} exist – for instance, Chin & Poulos (1991) recommends R_{fs}=0-0.5 and R_{fb}=0.9 while Chow (1986) modelled London Clay using R_{fs}=R_{fb}=0.9. Parametric testing of the effect of R_{fs} and R_{fb} will be conducted in section 5.2.

4.2 Example simulation outputs

The incrementally-obtained values of P and u for each node represent the load-displacement relationship for the node, as shown in Fig 9.1. Often, the pile load-displacement relationship is also plotted as shown in Fig 9.2, giving an indication of the pile capacity based on SLS and ULS. Fig 9.1 and 9.2 are examples of pile behaviour that are modelled by the new analysis tool using hypothetical soil conditions of: s_u=75kPa, α=0.6 and E_{soil} = 50MPa.

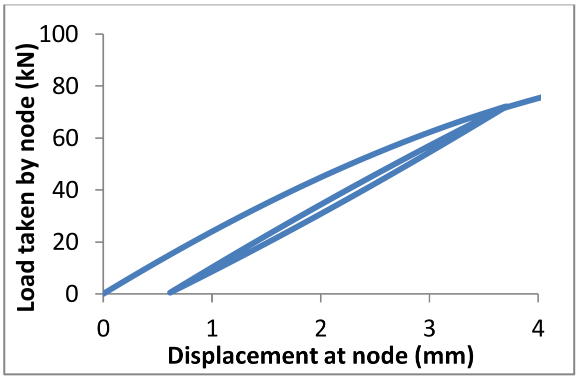

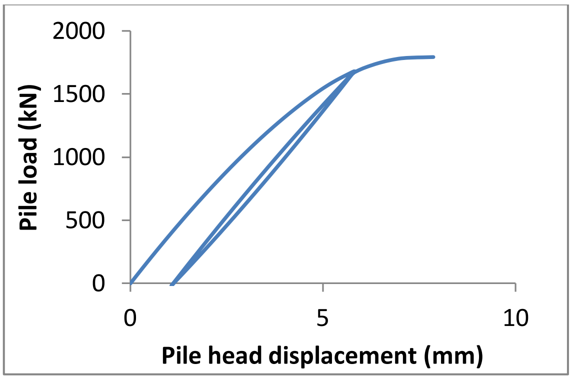

Note: Simulation of a 20m pile (0.3m radius) initially loaded to 1.7MN, then unloaded and reloaded to failure

Fig 9.1 Load-displacement curve of a pile shaft node

Fig 9.2 Load-displacement curve of a pile

Fig 9.3 shows the results of a simulation performed on a rafted foundation system using the same hypothetical soil conditions. For a foundation system involving rafts and pile groups, it is the differential deformation (and relative displacement) across the raft that governs thus Fig 9.3 shows the displacement pattern across the foundation. It also shows the proportion of ultimate pile capacity mobilised in each pile.

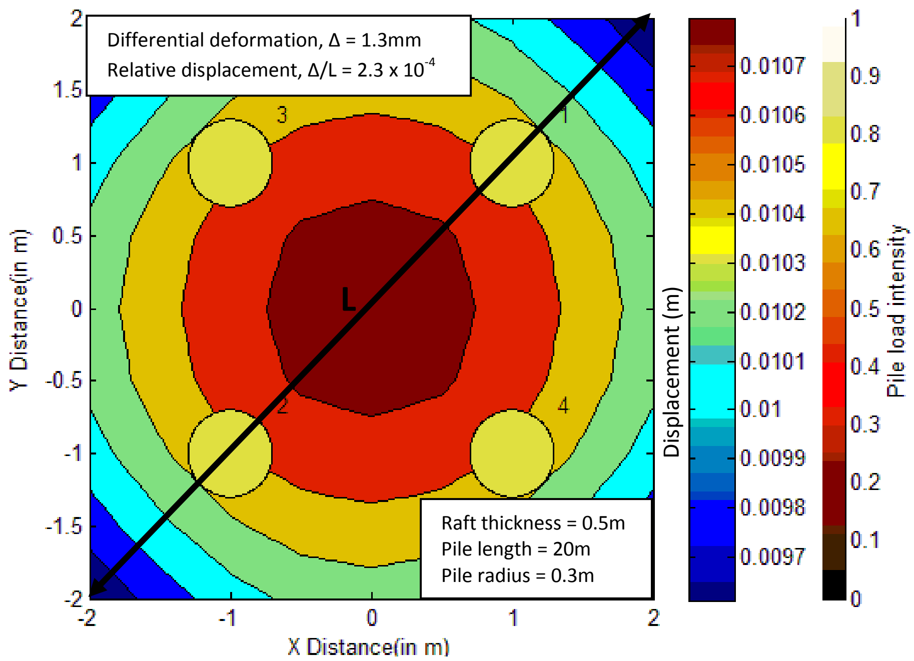

Fig 9.3: Example of simulation result for raft foundation system

5.0 Parametric testing of new analysis tool

In this section, a comparison of the non-linear cyclic load transfer solver to the elastic and elastic-plastic solvers in the current software is conducted. In addition, parametric testing of the new analysis tool will be conducted to determine the effect of various modelling parameters and soil parameters on the simulated soil behaviour. Finally, the new analysis tool will be validated against field pile tests. Unless otherwise indicated, soil conditions described in section 4.2 is used in these tests.

5.1 Comparison of various soil models

In this section, the non-linear cyclic load transfer solution is compared to elastic (Mindlin) and elastic-plastic solvers using piles loaded in soil conditions given in section 4.2.

A simulation of a 20m pile (0.3m radius) loaded to failure was performed and Fig 10 shows the load-displacement curve of a shaft node located 3m from the pile head for all 3 soil models. It can be seen from Fig 10 that, at low displacements, the 3 models behave similarly, but start to diverge at higher displacements. As the load increases, the elastic solution (incorrectly) assumes an infinite pile capacity with elastic soil behaviour. Both the elastic-plastic and non-linear load transfer models simulate a finite pile capacity, with large displacements at high loads. However, the 2 solutions differ as expected, with the non-linear model distinctly showing a gradual decrease of stiffness at loads below pile capacity, giving larger displacements while the elastic-plastic model remains elastic until the point of failure, where displacements increase suddenly. Since soil is a non-linear material with decreasing stiffness with strain, it is likely that the non-linear approach models soil behaviour more accurately. This is validated in later sections.

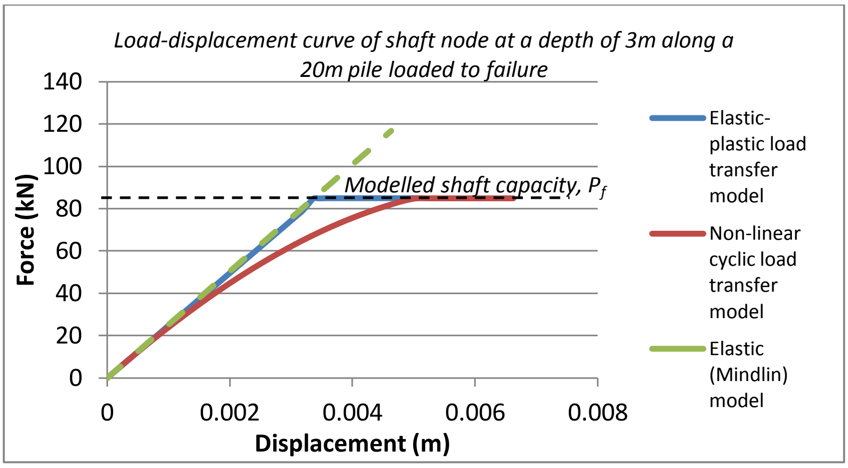

Fig 10: Comparison of soil models

A simulation was also performed on a foundation system comprising a 4x4m raft with 4 piles (0.6m diameter) as shown in Figs 11.1-11.4. All 3 models produce relatively similar differential deformations (within 10% of 1.2mm). Unsurprisingly, the deformations for the non-linear solution are generally larger and deviate from the other 2 models which corroborates well with the above. From Fig 11.3 and 11.4, the differential deformation is also shown to depend on the R_{fs} value, which affects how loads are distributed across the raft. This is discussed in section 5.2.

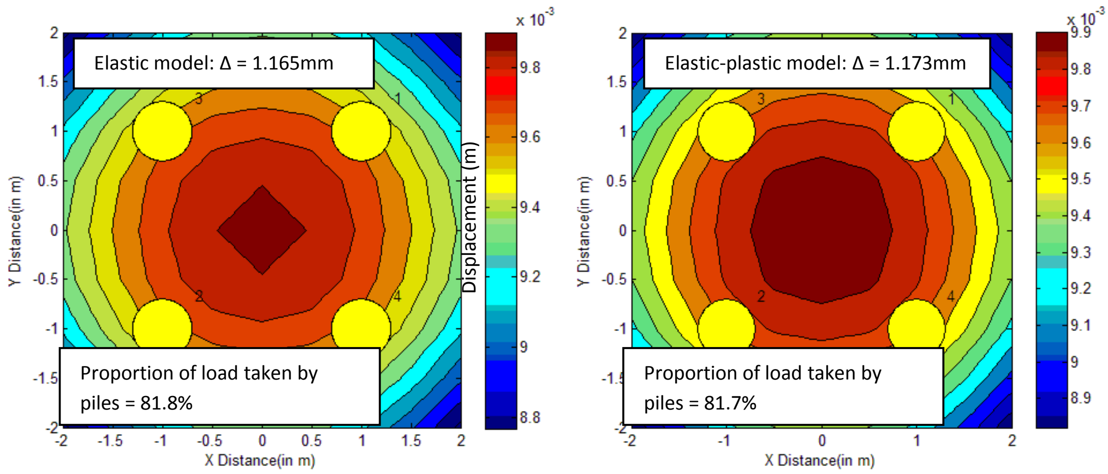

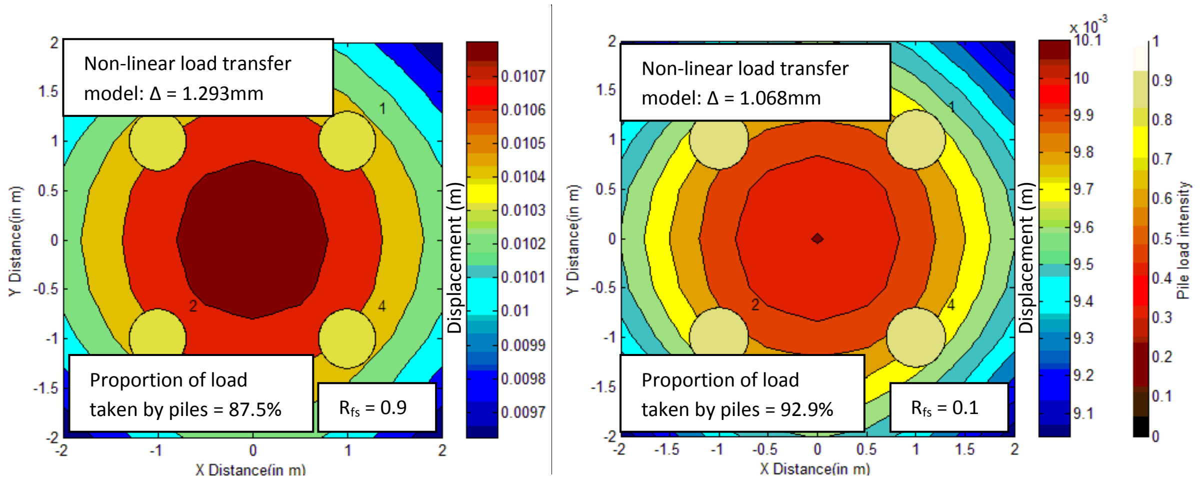

Fig 11.1(top left) – 11.4 (bottom right): Displacement plots of a 4m square raft with 4 piles with loads of 1.7MN applied to each pile head, simulated using various soil models as labelled

5.2 Effect of varying the hyperbolic curve-fitting constant (R_f)

As mentioned previously, the modelling parameter, R_f, in the new analysis tool can be adjusted to better fit test data. Thus, the effect of varying R_{fs} (shaft constant) is investigated in this section and the results can extrapolated for R_{fb} (base constant).

A simulation of a 20m pile loaded to failure was performed with R_{fs} varied from 0.1 to 0.9. From Fig 12, increasing R_{fs} appears to increase the rate of soil stiffness degradation (with increasing strain), resulting in larger deformations at higher values of R_{fs}.

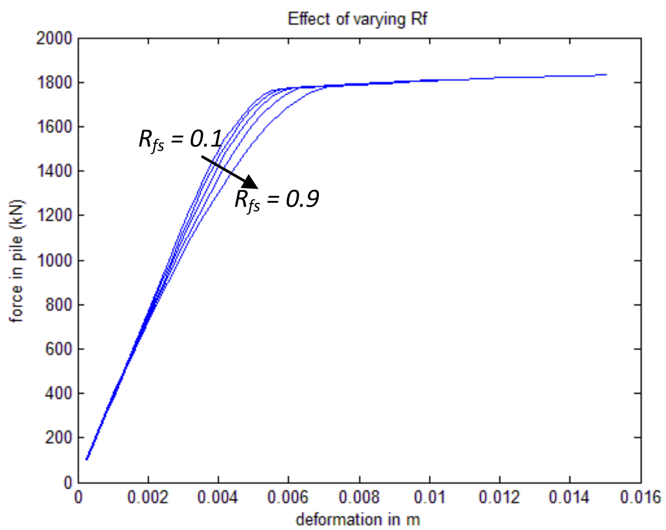

Fig 12: Effect of varying R_{fs} on the load displacement curve

Comparing Figs 11.3 and 11.4, a smaller value of R_{fs} models stiffer pile behaviour and a smaller differential deformation while increasing the proportion of load carried by the piles.

This is likely to be because stiffer behaviour means smaller deformations thus piles can take more load without suffering greater deformation so that the load is less well distributed across the raft.

The above study shows that the new analysis tool can give varying results depending on R_f. Thus, this shows the importance of using external pile test data to improve the accuracy of foundation simulations under various soil conditions.

5.3 Effect of changing soil stiffness (E_{soil}) and soil strength (s_u) with time

Case studies from various researchers (see section 2.4) indicate that pile stiffness and capacity can change with time due to changing soil stiffness and strength as a result of setup, consolidation and other soil mechanisms. Thus, in this section, the effect of changing soil stiffness and capacity is presented through parametric tests using the new analysis tool.

5.3.1 Effect of changing soil stiffness (E_{soil})

Research has shown that reloaded piles may increase in stiffness, possibly due to consolidation under initial loading. Two 20m piles of 0.6m diameter are simulated to study this effect. Initially, the piles are loaded to 1.6MN, unloaded and reloaded to 1.6MN. In the first pile (Fig 13.1), the soil stiffness remains constant while in the second case, (Fig 13.2), the soil stiffness, E_{soil}, is increased by 20% during reloading. From Fig 13, it is apparent that increasing soil stiffness reduces pile reload displacement thus, for soils in which stiffness increases with time, reused piles could be stiffer than originally intended, which may decrease the overall differential deformation of the foundations.

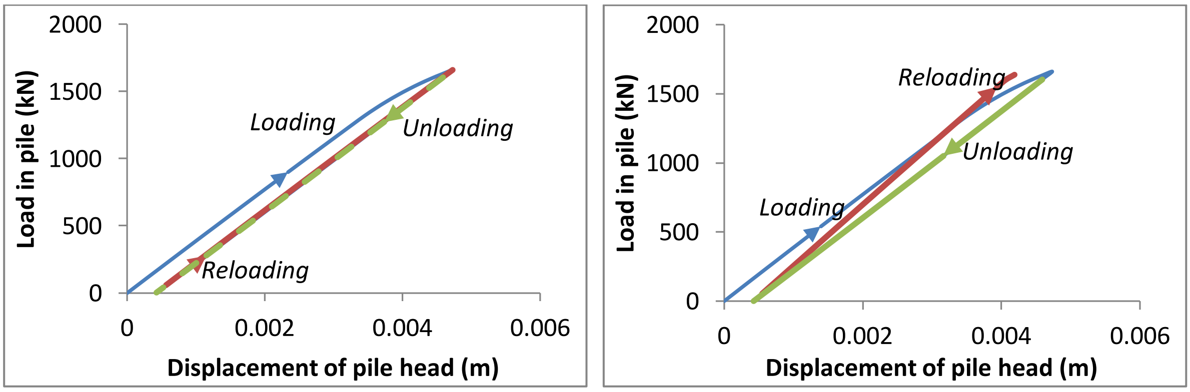

Fig 13: Load-displacement curves of pile with constant E_{soil} (13.1) and increased E_{soil} during reloading (13.2)

5.3.2 Effect of changing undrained soil strength (s_u)

Previous research has shown that the undrained soil strength (s_u) of soils (and thus pile capacity) could change after repeated cyclical loadings. An increase in capacity could be due to set-up, or a decrease due to strain softening of overconsolidated clays. To study this effect, two 20m piles of 0.6m diameter are simulated. Initially the piles are loaded to 1.8MN, unloaded and reloaded to 1.8MN. In the first pile (Fig 14.1), s_u remains constant while in the second pile, (Fig 14.2), s_u decreases by 10% during reloading, to simulate strain softening. From Fig 14, it is clear that a small decrease in s_u decreases pile capacity so that failure occurs at a smaller load. Thus, in soils where strain softening behaviour (or other mechanisms which may decrease s_u) is expected, it may be necessary to design reused piles with a higher safety factor for conservatism.

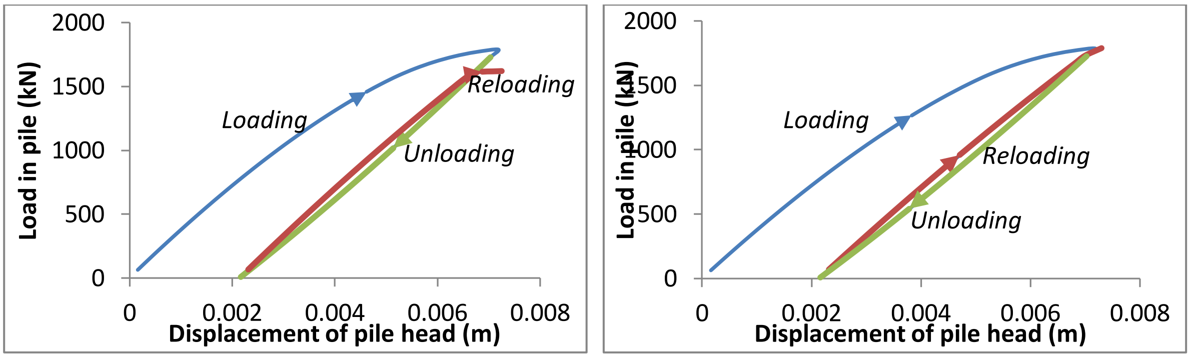

Fig 14: Load-displacement curves of pile with constant s_u (14.1) and decreased s_u during reloading (14.2)

In general, the above 2 studies demonstrate the importance of determining changing soil conditions for foundation reuse. Soil response may not always be predictable after a period of loading thus soil investigation or pile tests may be required to determine pile reuseability.

5.4 Effect of inhomogeneous soil conditions

Most soils are inhomogeneous and have increasing strength and stiffness with depth, which affects pile behaviour. In this section, the effect of non-uniform soil properties with depth is investigated using the new analysis tool.

5.4.1 Effect of variable s_u

Many soils experience increasing undrained shear strength (s_u) with depth due to consolidation. For instance, London Clay may have a typical undrained shear strength profile of s_u=120+9.2z kPa, which is used in this simulation.

To investigate the effect of variable s_u (compared to having a constant s_u), 2 piles of 0.5m radius and 20m length were modelled, one with a variable s_u (from above) and one with a constant s_u (s_u at the average depth of 10m = 212kPa), with α=0.6 and E_{soil}=88MPa. The 2 piles were first loaded with 1.5kN of load and then loaded to failure. From Fig 15.1, both load-displacement curves are quite similar at smaller loads. However, at higher loads, the 2 curves diverge, with the pile in variable soil showing less stiff behaviour, perhaps due to weaker soil near the pile head. Fig 15.2 shows the cumulative mobilised resistance along the pile due to shaft friction and base capacity during loading. Sharp increases in mobilised capacity are seen at the base of the piles due to the base capacity. At 1.5kN of load, both piles show a similar distribution of mobilised resistance (consistent with Fig 15.1) but at failure, mobilised resistance increases with depth (convex curve) for the pile in variable strength soil (soil strength increases with depth) but remains constant with depth for the pile in homogenous soil, as is expected.

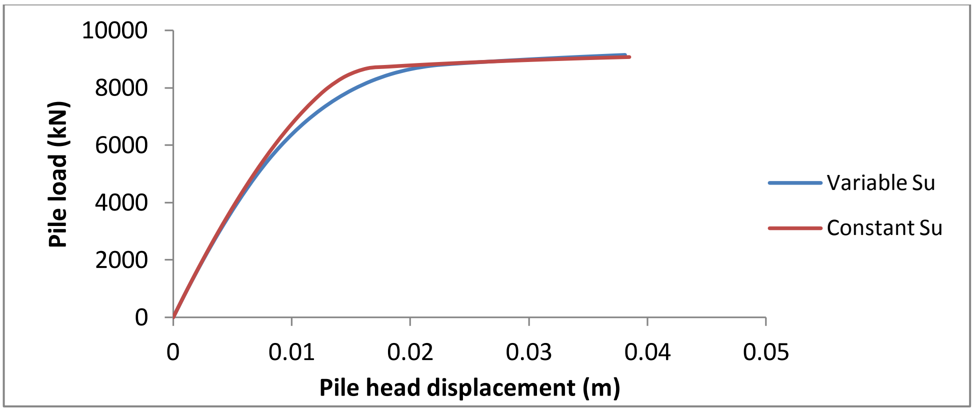

Fig 15.1: Effect of variable s_u vs. constant s_u on load-displacement behaviour of piles

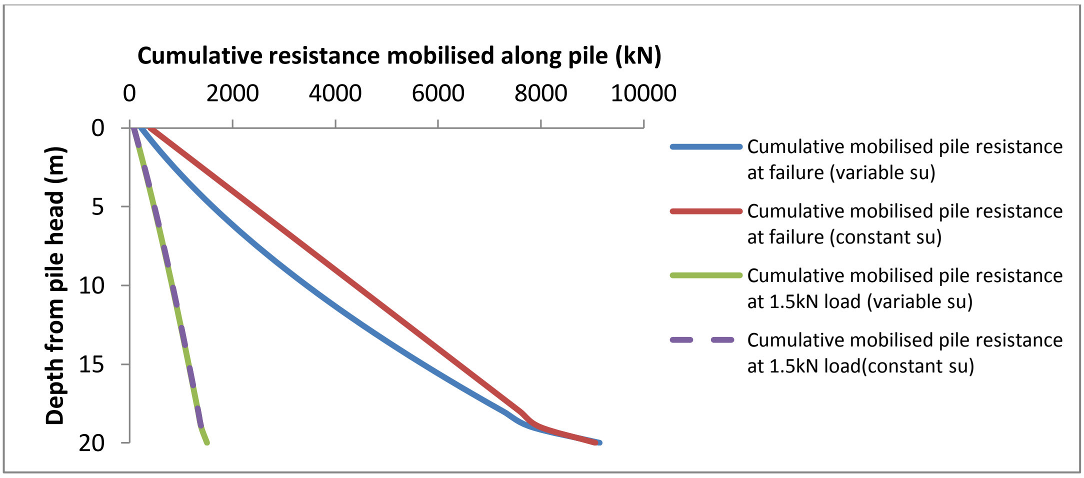

Fig 15.2: Effect of variable s_u vs. constant s_u on load taken along the pile

Given the less stiff behaviour of piles driven in soils with inhomogeneous strength, it is important to know the undrained strength profile and not just the average, to prevent unconservatism.

5.4.2 Effect of variable E_{soil}

As with s_u, soil stiffness tends to increase with depth due to consolidation. For instance, London Clay has a typical distribution of E_{soil}=36+5.2z MPa (Leung 2010). To investigate the effect of variable E_{soil}, 2 identical piles of 0.5m radius and 20m length were modelled and loaded, one with a variable E_{soil} (from above) and one with a constant E_{soil} (E_{soil} at the average depth of 10m=88MPa), keeping s_u and α constant at 212kPa and 0.6 respectively.

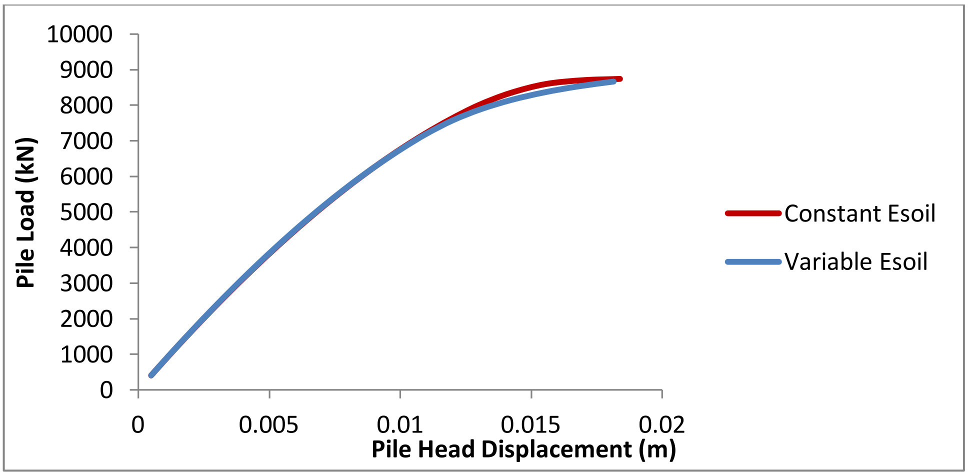

Fig 166.1: Effect of variable E_{soil} vs. constant E_{soil} on load-displacement behaviour of piles

From Fig 16.1, it is apparent that a variable E_{soil} has little effect on pile behaviour until at loads near capacity where the pile in variable soil displays marginally lower stiffness. The behaviour of shaft displacement and mobilised shaft resistance (for each pile element) along the length of the pile when loaded to 2MN is shown in Fig 16.2 and 16.3. From Fig 16.2, it is seen that, moving away from the pile head, the displacements of both piles diverge, with the pile in variable soil showing stiffer behaviour due to stiffer soil at greater depth.

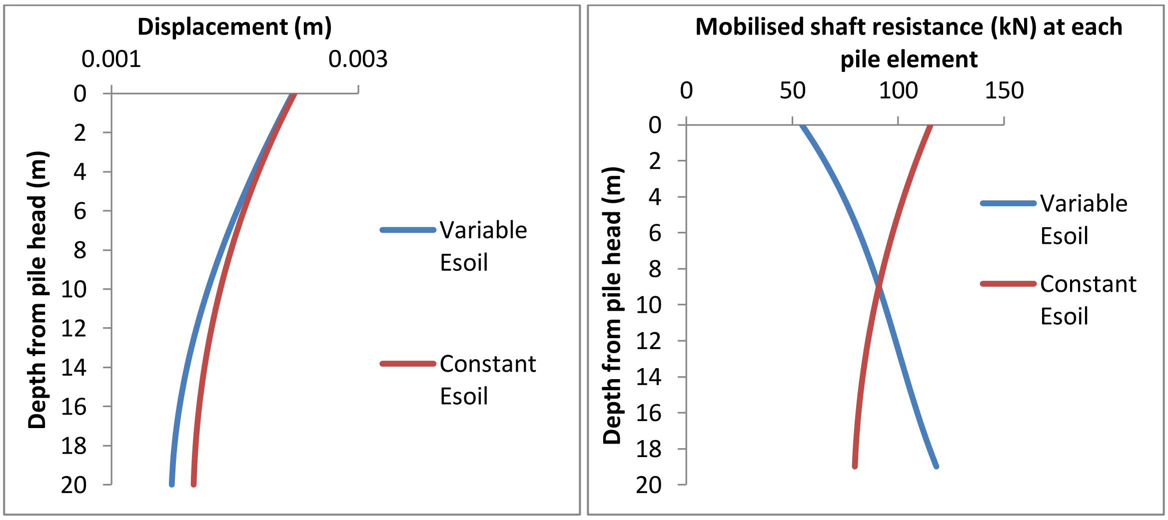

Fig 16.2, 16.3: Effect of variable E_{soil} vs. constant E_{soil} on displacement (left) and shaft resistance (right) along the length of the pile under a total load of 2MN. Note that base resistance is omitted from 15.3 for clarity.

From Fig 16.3, it is seen that the mobilised shaft resistance along both piles differ. For the pile in homogenous soil, resistance decreases with depth as the load is transferred from the pile head (where the load is applied) to the toe, hence greater load is carried near the pile head. For the pile in variable soil, the converse occurs, possibly as deeper soils are stiffer and thus require less displacement to mobilise a greater resistance.

This shows that homogeneity of soil stiffness has little effect on the load-displacement behaviour of the pile at lower loads as the load is effectively redistributed to achieve approximately the same pile head displacement (and thus overall stiffness). At higher loads, soil stiffness homogeneity may have an effect on the pile behaviour thus assuming soil homogeneity may not be conservative.

5.5 Effect of raft thickness

In foundation design, differential deformation is often the limiting factor. In order to reduce differential deformations, a pile group is often rafted to increase the foundation stiffness and reduce differential deformations. The raft may also carry some load and thus reduce pile design requirements. In this section, the effect of raft thickness on foundation performance is investigated using the new analysis tool.

A foundation consisting of a square raft and four 0.6m diameter 20m piles is modelled (Fig 17.1). A total load of 8MN is applied to the foundations, with 2MN applied at each of the pile heads. Raft thickness is slowly increased from 0m (no raft, differential deformation of 2.5mm) to 2m and the proportional reduction in differential deformation (from a case with no raft) is plotted on Fig 18.1. Fig 18.2 shows the effect of raft thickness on the proportion of total load taken by piles and raft.

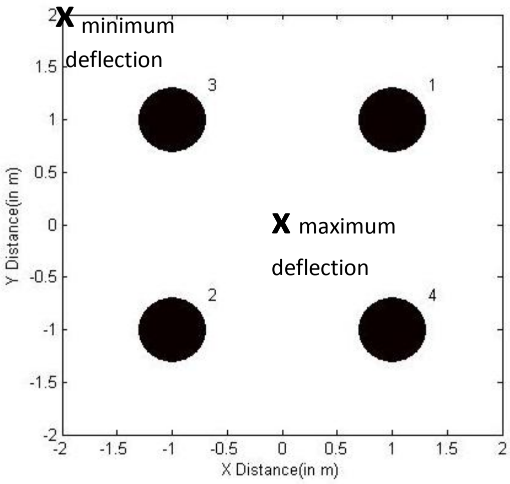

Fig 17: Modelled foundation with square raft (4x4m) and 4 piles

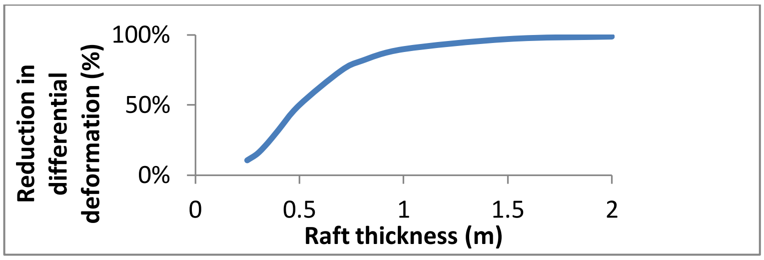

Fig 18.1: Effect of raft thickness on differential deformation

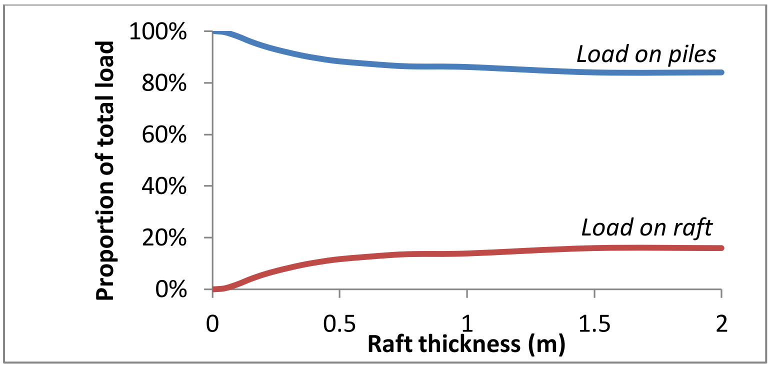

Fig 18.2: Effect of raft thickness on load taken by piles

From Fig 18.1, it is clear that the raft reduces the differential deformation significantly. At large raft thicknesses, the foundations are effectively rigid with negligible differential deformation. Fig 18.2 shows that as the raft thickness increases, the raft takes a greater proportion of total load though this eventually tails off, indicating that there is a limit to the amount of load redistributed to the raft. Thus, having a raft can decrease differential deformation significantly and reduce loads on piles to a small extent.

5.6 Validation of non-linear load transfer solution against field test

In order to validate that the non-linear load transfer solution models soil behaviour more accurately then the elastic and elastic-plastic approaches, the 3 approaches are compared against a field measurements of a maintained load test (MLT) in the work by Powell & Brown (2006) and Powell & Skinner (2006). The test was performed on pile T28 (in London Clay) which had an effective length of 6m and was loaded to failure.

Pile performance is simulated using all 3 soil models with R_{fs} = 0.5 and R_{fb} = 0.9 using the given s_u=75+11.7z kPa and α=0.6. A typical soil stiffness profile for London Clay (E_{soil}=36+5.2z MPa) is used as site conditions were not specified. A comparison of the simulated load-displacement curves to the field test measurements is shown in Fig 20.1.

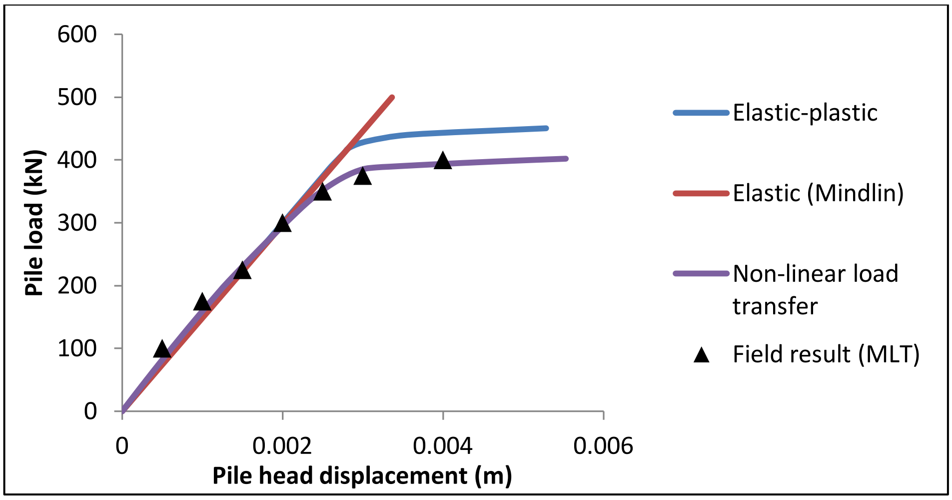

Fig 20.1: Comparison of 3 soil models to T28 field measurements

It is apparent that all 3 soil models simulate the actual pile performance well at low displacements when soil is behaving approximately linearly. However, as expected, the 3 solutions start to diverge at higher displacements, when soil behaves non-linearly. The non-linear load transfer solution shows good agreement with the field measurements while the other 2 approaches diverge from the field results. This can be attributed to the fact that the elastic solution does not consider soil non-linearity while the bilinear solution only considers non-linearity at failure.

To further validate the new analysis tool which uses the non-linear load transfer solution, more comparisons against field measurements are undertaken. Figs 21.1 and 21.2 show comparisons of numerical simulations (from new analysis tool) against field measurements from pile tests (on closely-located 7m piles T45A and T44 respectively) undertaken by Fernie et al. (2006) at a London Clay site at Chattenden where s_u=20+17.14z kPa. Pile stiffness is modelled as typical London Clay (E_{soil}=36+5.2z MPa) and α=0.5 is assumed.

From Fig 21.1, the numerical simulation agrees well with field results at displacements below the ultimate capacity but does not simulate the peak capacity. Post-peak, the simulated ultimate pile capacity agrees well with the field measurements.

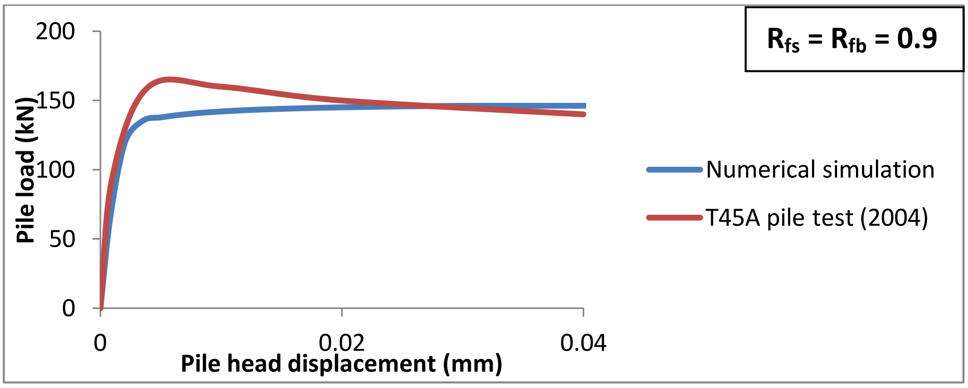

Fig 21.1: Comparison of numerical simulation against field test on pile T45A

From Fig 21.2, the numerical simulation displays much stiffer behaviour than the T44 pile test from 2002 (T45A was taken in 2004). A possible reason for this discrepancy could be that the 2002 T44 test was conducted on softer soil than modelled but consolidation may have occurred between 2002 and 2004, resulting in stiffer soil (for the T45A test) well-approximated by E_{soil}=36+5.2z MPa. Nonetheless, the simulated ultimate capacity for T44 at failure agrees well with the field capacity of T44.

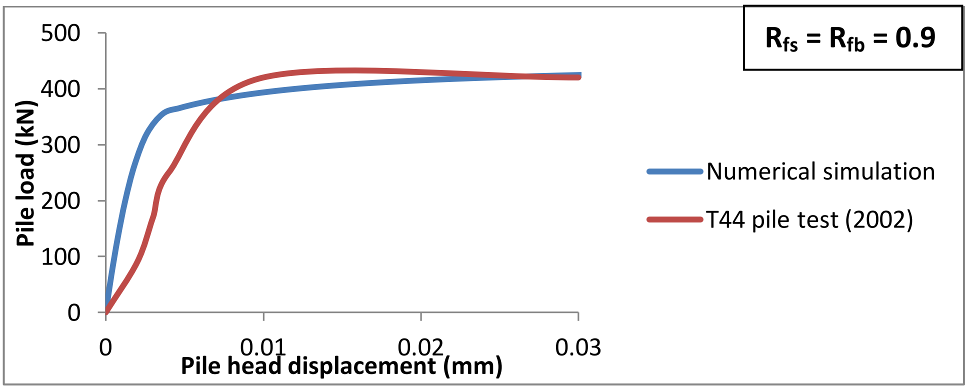

Fig 21.2: Comparison of numerical simulation against field test on pile T44

From these pile tests, the new analysis tool appears to model foundation performance more accurately than the elastic and elastic-plastic approaches at high strains if the appropriate value of R_{fs} is used and in general shows good agreement with field measurements. It is noted that Chow (1986) recommends R_{fs} = 0.9 for London Clay.

6.0 Simulation of Bevis Marks foundation reuse site

As the CUED has a research interest in the Bevis Marks foundation reuse project, a key objective of this research was to simulate the Bevis Marks foundations using the 2 existing approaches (elastic and elastic-plastic models) as well as the new analysis tool and compare the simulation results to field data. Key background information was provided in section 1.2. This section describes simulation parameters as well as simulation results.

6.1 Simulation parameters

The following describes the parameters and data used to model the Bevis Marks foundations. Original building loads are modelled using all 3 analysis methods while the cyclic behaviour during unloading (demolition) and reloading (construction of new building) is modelled using only the new analysis tool.

- **Ground conditions modelled**
  - Foundations are located entirely in London Clay hence only soil properties in this layer are relevant.
  - From SCL, α=0.45, N_c=7.5 and s_u=120+9.2z_{clay}kPa. The undrained strength profile is assumed to remain unchanged during the lifetime of the piles.
  - Soil stiffness profile is assumed to be typical of London Clay (E_{soil}=36+5.2z MPa) as no site-specific values were available.
- **Foundations modelled**
  - Existing piles: modelled as under-reamed piles with enlarged base with 4 times the cross-sectional area as at the pile head
  - New piles: modelled as straight-shafted piles
  - Raft thickness: 0.5m for original building, 1.5m for new building
- **Loads modelled (see Appendix 3)**
  - Original loads: Pile loads for the original Bevis Marks building is provided by SCL's preliminary assessment as "proven" loads. It is assumed the original loads are completely unloaded during demolition.
  - New building loads: New building loads were provided by Waterman.
- **Modelling parameters** (see Fig 22 for finite element node map)
  - R_{fs} = R_{fb} = 0.9 (recommended by Chow (1986) for London Clay)
  - Size of raft element = 8x8m, pile element length = 1m

6.2 Simulation results and comparison to field data

6.2.1 Comparison of results across the 3 soil models

The results of the 3 simulations are given in Table 1. It can be seen that all 3 simulations give similar results (within 10%) with the non-linear load transfer solution giving higher settlements and a higher differential settlement. The simulated differential settlements (about 10-13mm) for the original building and new building (about 33mm) are quite low and give small relative displacements which will not result in building damage (Appendix 1).

Solution	Original building				New building	
	Differential settlement (mm)	Max. settlement of raft (mm)	Min. settlement of raft (mm)	Relative displacement	Differential settlement (mm)	Relative displacement
Linear (Mindlin)	10.5	30.1	19.6	$0.180.10^{-3}$	-	-
Elastic-plastic load transfer	10.8	30.7	19.9	$0.186.10^{-3}$	-	-
Non-linear load transfer	12.4	33.5	21.1	$0.213.10^{-3}$	33.4	$0.476.10^{-3}$

Table 1: Differential settlement of old Bevis Marks building using numerical analysis

Fig 23 shows a comparison of the load-displacement curve of pile 34 for all 3 solutions, further validating that all 3 models give similar results with the non-linear load transfer solution deviating from the elastic-plastic and elastic solutions at higher displacements due to the non-linearity of soil modelled.

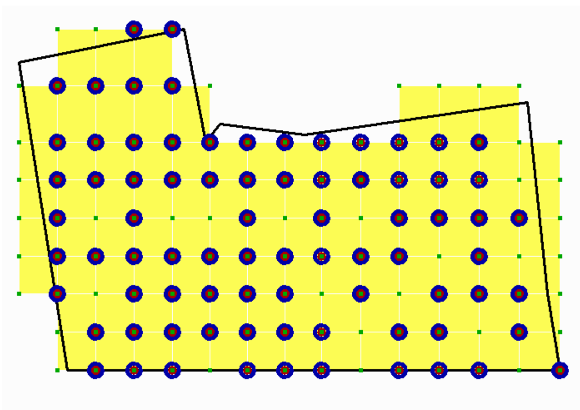

Fig 22: Finite element node map of Bevis Marks foundations

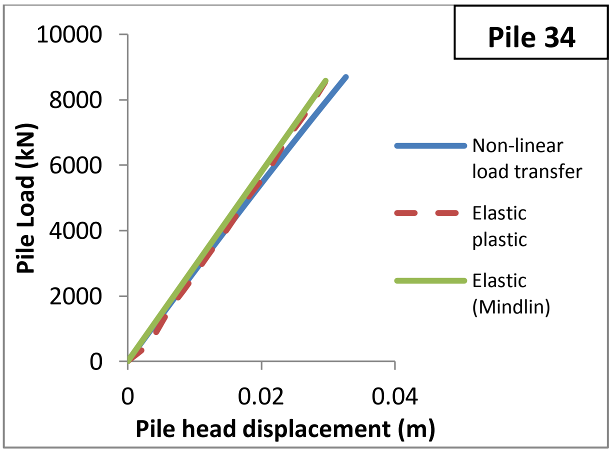

Fig 23: Load-displacement curve (pile 34)

6.2.2 Analysing the foundation performance loading and reloading

The simulated deformation (from new analysis tool) plots of the Bevis Marks foundations due to original and new building loads are shown in Figs 24.1 and 24.2 respectively. They also show the amount of load carried by each pile. Both plots predict that the highest deformations tend to occur around the centre of the raft with deformation decreasing towards the edges as the raft is not fully rigid. In addition, piles near the centre of the raft tend to be the most heavily loaded. From the plots, it can be seen that the new building has a load much more concentrated in the centre (as seen from the highly loaded piles near the centre and less highly loaded piles at the edges), near the point of greatest displacement so that the differential deformation is much higher than for the old building (33m vs. 12mm from Table 1). For the old building, it appears that the pile loads (and thus displacements) are more uniform (zone of largest displacement is much larger for the old building).

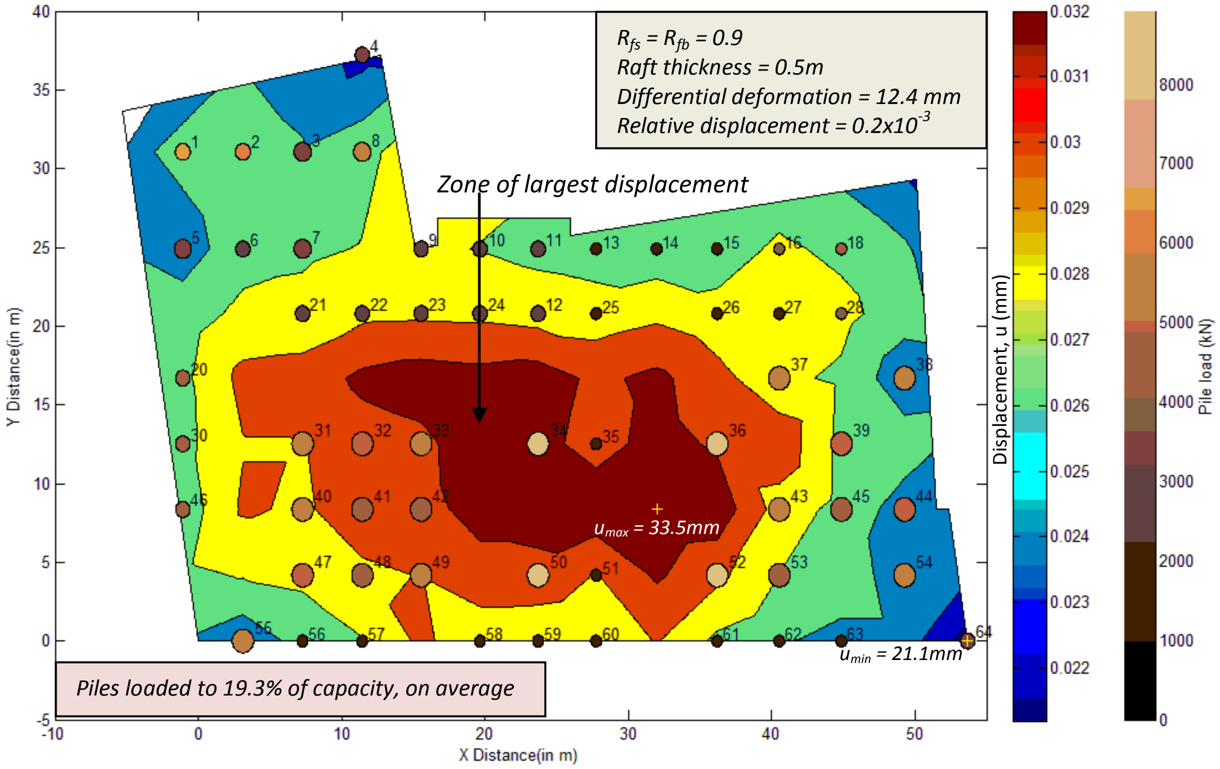

Fig 24.1 Simulated Bevis Marks deformation plot due to original building loads (non-linear load transfer)

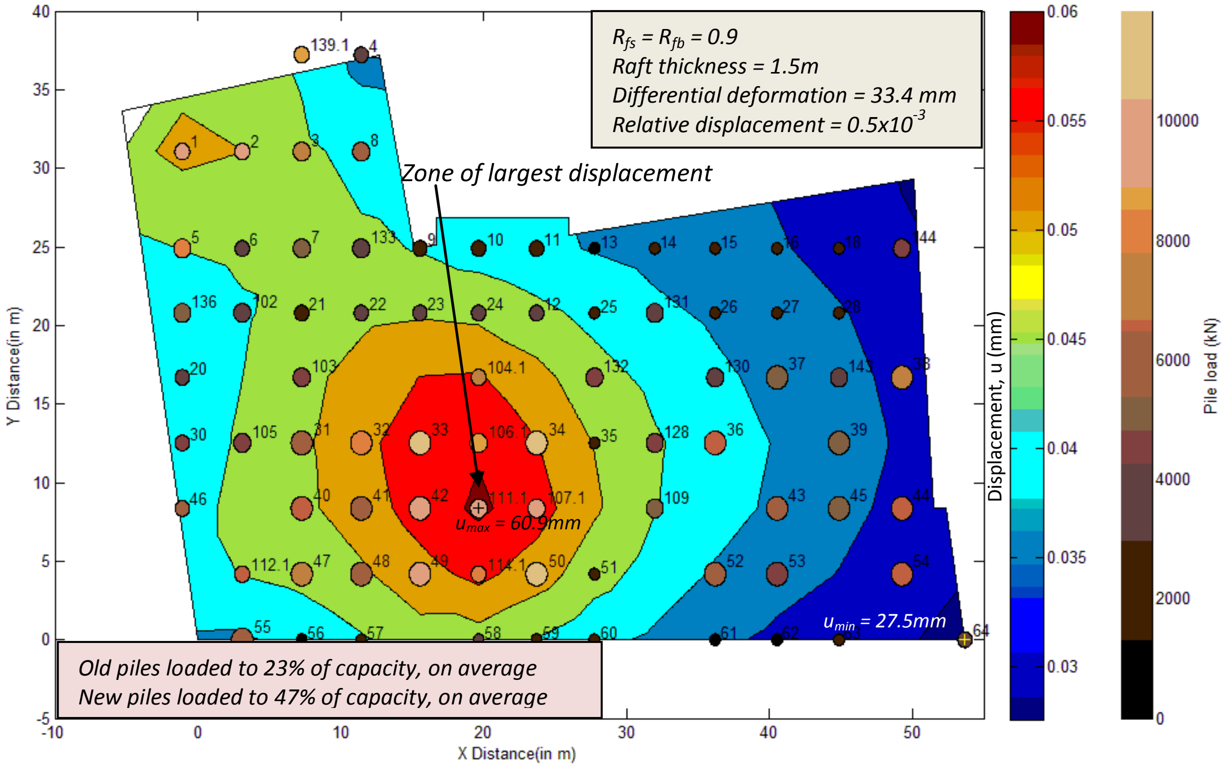

Fig 24.2 Simulated Bevis Marks deformation plot due to new building loads (non-linear load transfer)

Table 2 shows the proportion of total load carried by the piles (old and new) and raft for both the original and new Bevis Marks buildings (from simulation using new analysis tool). It also shows the proportion of capacity mobilised by each foundation component. For the old building, it is seen that, on average, piles are loaded to less than 20% of their capacity, giving an average safety factor (FoS) of 5.2, which is very conservative. In general, for the original building, no pile is loaded beyond 36% of its ultimate capacity (average of 15%), giving a conservative minimum FoS of 2.75.

Foundation component	**Original building**			**New building**		
	% of total load on foundation[1]	% of capacity mobilised[2]	Factor of Safety	% of total load	% of capacity mobilised	Factor of Safety
Raft	0	0	-	0	0	-
Old piles	100	19.3	5.2	72.5	23.2	4.31
New piles	-	-	-	27.5	46.1	2.17
All piles	*100*	*19.3*	*5.2*	*100*	*26.9*	*3.72*

Table 2: Simulated distribution of loads and mobilised capacities for original and new Bevis Marks buildings

[1] % of total load of foundation refers to the proportion of the total load on foundation that is carried by that foundation component

[2] % of capacity mobilized refers to the proportion of capacity (of foundation component) that has been mobilized.

For the new building, old piles carry most of the load (72.5%) with the new piles carrying the rest (27.5%), which is expected as there are many more old piles than new piles. However, on closer inspection, it is seen that old piles appear to mobilise only 23.2% of their capacity (FoS = 4.31 which is very conservative) compared to that of new piles (46.1% giving a FoS = 2.17 which is acceptable). It is possible that the capacity of reused piles is less certain due to possible loss of integrity and pile strength thus requiring a much higher factor of safety.

Unusually, it is found from Table 2 that the raft does not carry a significant amount of load, which may suggest that it is redundant in terms of carrying capacity. To investigate the redundancy of the raft, a second simulation was performed but with a negligibly thin raft (0.01m), with results shown in Table 3. As expected, the thinner raft did not carry much load. A comparison of differential deformations for the foundations under the old building load shows that the 0.5m raft reduces the differential deformation by 17% (from 14.9mm to 12.4mm). For the new building, it was found that the additional 1.0m transfer slab (which triples the current slab thickness) only reduces the differential deformation by another 16% (39.6mm to 33.4mm). Given that the transfer slab increases the cost and embodied energy of the reuse project, a cost-benefit analysis could be conducted to determine the necessity of the slab.

Simulated raft thickness (m)	**Differential deformation Δ (mm)**	
	Old building	New building Δ
0.01	14.9	40.9
0.5	12.4	39.6
1.5	-	33.4

Table 3: Differential settlements for various raft thickness at Bevis Marks

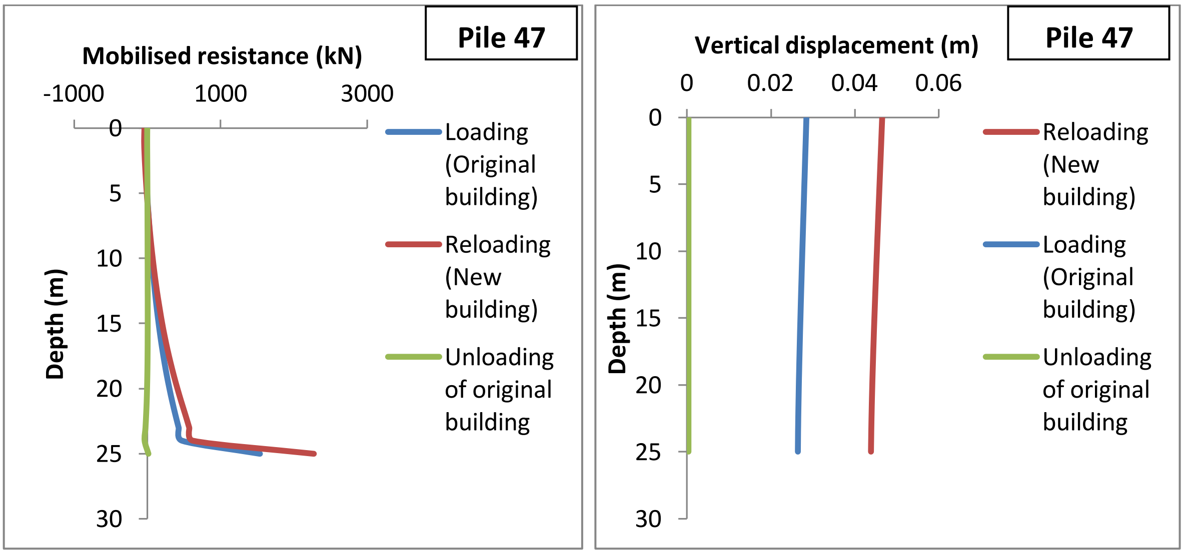

Fig 25.1 and 25.2: Variation of mobilised (shaft and base) resistance (left) and displacement (right) along pile length for pile 47 (existing pile) from non-linear load-transfer solution

Fig 25.1 and 25.2 show the variation of mobilised shaft (or base) resistance and displacement with depth for a typical reused and under-reamed pile, pile 47 during the load-unload-reload process. From Fig 25.1, it is seen that mobilised pile resistance increases sharply towards the enlarged base, as most of the load is carried toward the base of the pile. Negative shaft resistance is mobilised toward the pile head during loading and reloading. It is possible that this negative shaft resistance is due to the softer soil surround the pile which displaces vertically downwards more than the pile head, inducing negative shaft resistance near the pile head. Comparatively, stiffer soil near the pile toe does not displace as much as the pile itself, inducing positive shaft resistance.

During demolition (i.e. unloading), Figs 25.1 and 25.2 show that pile 47 appears to be unloaded completely with negligible residual displacement. This indicates that the pile behaviour during the load-unload process for the original building remains approximately elastic (which is recovered during unloading) at relatively low strains (and low loads proportional to pile capacity) to maintain a high safety factor. Fig 25.2 indicates that, on reloading, the foundation experiences much higher displacement than on loading, which agrees with results from Table 1. On reloading, pile 47 also takes on more load than during loading, from Fig 25.1.

6.2.3 Comparison of numerical simulation to field data

Optical fibre cables were used to determine the relative strain change (and thus relative displacement) along pile 47 during demolition (unloading). The strain measurements were taken in August 2011 and October 2011, during which approximately 70% of the original Bevis Marks building was demolished. The strain change (and relative vertical deformation) was taken relative to the base of the cables (at 17m depth) and 2 sets of readings were taken and compared. This was compared to the results of the numerical simulation using the new analysis tool and shown in Fig 26. It is seen that the numerical simulation overestimates the relative deformation along the pile length but in general agrees well with one set of the fibre optics data (set 2).

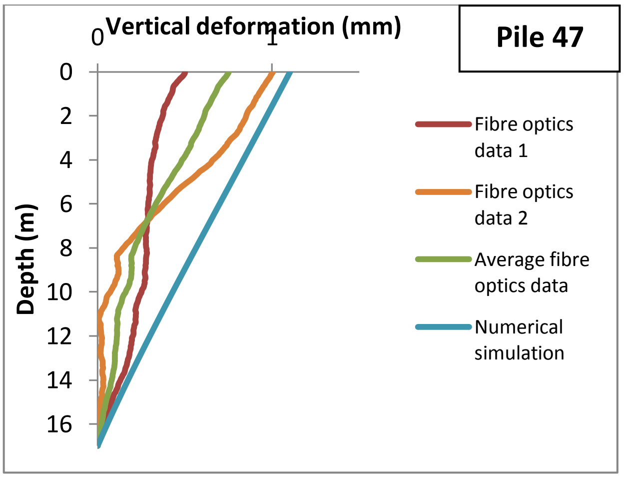

Fig 26: Comparison of fibre optics data to numerical analysis – relative vertical deformation (to 17m depth) during unloading with depth for pile 47

The deviation of the numerical simulation from the fibre optics data could be attributed to the inaccuracies in modelling and instrumentation. For instance, in modelling the Bevis Marks site, soil parameters could have been incorrectly assumed (e.g. it is assumed that the soil stiffness profile is typical of London clay) or modelling parameters (e.g. R_{fs} = 0.9) could have been incorrectly defined. In addition, fibre optics strain measurement is a relatively new technique and is not perfectly accurate. This is seen in Fig 26, where both sets of field data also deviate. Furthermore, during demolition, the fibre optic cables in pile 47 were also slightly damaged, which may have affected the accuracy of field data. Further investigation using more reliable instrumentation techniques and more accurate soil data is needed to verify the accuracy of the fibre optics and simulation results.

Pile 38 was also similarly instrumented with fibre optic cables but due to severe cable damage during demolition, the field data was deemed unsuitable for comparison.

7.0 Risk Assessment of Research Project

Prior to this research, a risk assessment was conducted to mitigate potential hazards in this project. A post-project evaluation of the risk assessment is found in Appendix 4.

8.0 Conclusion

The following conclusions can be drawn from this research:

- Foundation reuse is increasing in popularity and motivated by ground congestion and sustainability. However, there is much uncertainty in the behaviour of reused piles thus there is an imperative to develop software to model pile reuse behaviour.
- The current Cambridge foundation software utilises finite element meshing to model foundation systems using elastic and elastic-plastic soil modelling approaches which are accurate at low strains but do not model non-linear soil behaviour at high strains accurately.
- This research project developed a novel analysis tool for the Cambridge foundation software utilising a non-linear cyclic load transfer approach presented by Chin & Poulos (1991) and Chow (1986).
- The new analysis tool has been demonstrated to agree well with elastic and elastic-plastic approaches at low strains but at high strains it can also model non-linear soil behaviour. Numerical analysis results from the new analysis tool have been shown to agree well with field tests on single piles.
- To further this research, parametric tests were conducted using the new tool to demonstrate that expected pile behaviour is simulated. Parametric tests were also conducted to show how simulated pile behaviour varied with changing modelling parameters.
- Finally, the new tool was demonstrated on the Bevis Marks foundation reuse project in London. Numerical analysis indicates that the original and new Bevis Marks buildings have acceptable differential deformations, which have been reduced due to the raft. Interestingly, during loading, the piles mobilise negative shear resistance near the pile head, possibly due to soft clay at shallower depths which displace more

than the pile. During unloading, pile deformation is elastically recovered due to relative low strains and high safety factors. Results of the simulation largely agree with field data from optical fibre cables, though further work needs to be done to verify the accuracy of the simulation.

9.0 Recommendations for Future Work

Based on the above non-linear cyclic load transfer solution the following work is recommended to further this research:

- The tool can be used to simulate more foundation reuse sites in various soil conditions and results of the numerical analysis can be compared to field data to further validate the new analysis tool. This will help build a database of recommended modelling parameters for various soil conditions and help improve the accuracy of numerical analysis.
- The software can also be compared against currently available software to gauge performance in terms of robustness, speed and accuracy. This work is currently being executed by researchers in the CUED.
- Given the active research and application of geothermal piles (Leung, 2010), this analysis tool can be further developed to incorporate thermal effects in energy piles so as to aid in the design of geothermal piles.

10.0 Acknowledgements

I would like to thank my research supervisor, Prof Kenichi Soga, for his continuous support and guidance throughout the research process. I would also like to thank Dr. Jize Yan who has mentored me throughout the process. I would also like to thank the following members of the Geotechnical Research Group who have helped in my project in one way or another: Echo Ouyang, Zili Li, Fuxue Sun and Yoshiharu Asaka.

11.0 References

[1] *Reuse of foundations for urban sites (RuFUS): A best practice handbook*

[2] *RuFUS: Proceedings of the International Conference*

[3] Vaziri, M. & Windle, J. (2006). “Strategy for the reuse of existing piles: Case study at Belgrave House, London”. *Proceedings of the International Conference on Reuse of Foundations for Urban Sites*, Watford. pp. 47-58.

[4] Stamatopoulos, A. C. & Stamatopoulos, C. A. (2006). “The new Acropolos Museum of Athens”. *Proceedings of the International Conference on Reuse of Foundations for Urban Sites*, Watford. pp. 287-295.

[5] Powell, J. J. M. & Skinner, H. D. (2006). “Capacity changes of bored piles with time”. *Proceedings of the International Conference on Reuse of Foundations for Urban Sites*, Watford. pp. 237-248.

[6] Powell, J. J. M. & Brown, M. J. (2006). “Statnamic pile testing for foundation reuse”. *Proceedings of the International Conference on Reuse of Foundations for Urban Sites, Watford*. pp. 223-236.

[7] König, F., Grabe, J., Franke, J. & Woldt, J. (2006). “Load bearing behaviour of an existing pile foundation and changes with time”. *Proceedings of the International Conference on Reuse of Foundation for Urban Sites*, Watford. pp. 199-211.

[8] Fernie, R., Bourne-Webb, P., Shotton, P. & Tester, P. (2006). “Observations of pile-to-pile and pile-cap interaction, at a well calibrated RuFUS test site”. *Proceedings of the International Conference on Reuse of Foundations for Urban Sites*, Watford. pp. 187-198.

[9] Leung, Y. F. (2010). “Foundation optimisation and its application to pile reuse”. University of Cambridge, Cambridge.

[10] Mindlin, R. D. (1936). “Force at a point in the interior of a semi-infinite solid”. *Physics* 7, 195 - 202.

[11] Klar, A., Spasojevic, A.D. & Soga, K. (2004). “Continuum solution of lateral loading of large pile groups”. *Technical Report TR334, CUED/D.* University of Cambridge, Cambridge.

[12] Klar, A., Vorster, T. E. B., Soga, K. & Mair, R. J. (2007). Elastoplastic solution for soil-pipe-tunnel interaction. *Journal of Geotechnical and Geoenvironmental Engineering, ASCE 133*. No. 7, 782-792.

[13] Skempton, A.W. (1951), "The Bearing Capacity of Clays," Proc. Building Research Congress, vol. 1, pp. 180-189.

[14] Zienkiewicz, O. C. & Taylor, R. L. (2005). "The finite element method for solid and structural mechanics". *Sixth edn, Oxford: Butterworth-Heinemann*.

[15] Randolph, M.F. & Wroth, C.P. (1978). "Analysis of the deformation of vertically loaded piles". *Journal of Geotechnical Engineering Division.* ASCE. 104 No. 12. p1465-1488.

[16] Kraft, L. M., Ray, R. P. & Kagawa, T. (1981). "Theoretical t-z curves". *Journal of Geotechnical Engineering Division*. ASCE. 107 No. 11. p1543-1561.

[17] Chin & Poulos. (1991). "A "T-Z" approach for cyclic axial loading analysis of single piles". Computers and Geotechnics 12 p289-320.

[18] Chow, Y. K. (1986). "Analysis of vertically loaded pile groups". *International Journal for Numerical and Analytical Methods in Geomechanics* 10. p59-72.

[19] "6 Bevis Marks, London" 51^{o}51'49.92" N and -0^{o}07'93.68" E (June 2008). *Google Maps.* Retrieved October 17, 2011 from https://maps.google.com/

[20] Wembley Laboratories Limited (1980). "Site Investigation Report- Bevis Marks, London".

[21] Soil Consultants Ltd (2009). "Preliminary Assessment of Existing Piled Foundation and Potential for Re-Use – 6 Bevis Marks, London EC3A".

[22] Waterman (2010). "6 Bevis Marks Stage D Report, Volume 2: Structural Design".

[23] Waterman (Apr 2010). "6 Bevis Marks Project: Piling Layout (drawing)".

[24] Waterman (Apr 2010). "6 Bevis Marks Project: Piling Schedule".

[25] Geotechnical and Environmental Research Group, Department of Engineering, University of Cambridge. "Method Statement: Installation of fibre optical sensors, Marks Bevis – City of London".

[26] Yan, J., Wang, F., Ouyang, E., Elshafie, M. & Soga, K. (2011). "Optical Fibre Monitoring Project at Bevis Marks". University of Cambridge, Cambridge.

[27] Wang, F., Yan, J., Sun, F., Elshafie, M. & Soga, K. (2011). "Pile performance report for building demolition in Bevis Marks 6." University of Cambridge, Cambridge.

[28] Boscarding, M.D. and Cording, E.G. (1989). "Building Response to Excavation-Induced Settlement". *Journal of Geotechnical Engineering*. ASCE. 115;1;1-21.

[29] Bolton, M.D. & Haigh, S.K. (Jan 2011). "Cambridge University Engineering Department Supplementary Databook Module 4D5: Foundation Engineering".

Appendix 1: Effect of relative displacement on building damage

According to Bolton & Haigh (2011), for L, the length of a building segment with constant sagging/hogging, the differential displacement is Δ, the maximum settlement of the deformed segment as shown in Fig A.1 and relative displacement is Δ/L.

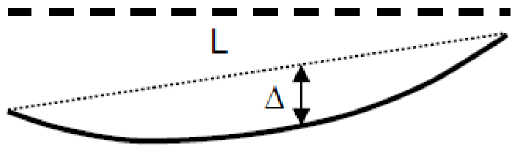

Fig A.1: Illustration of differential deformation and relative dispalcement

Boscardin and Cording (1989) define categories of building damage due to relative displacement is as shown in Table A.1.

Category	Relative displacement range	Amount of damage
0	$\Delta/L \le 0.5 \times 10^{-3}$	Negligible
1	$0.5 \times 10^{-3} \le \Delta/L \le 0.75 \times 10^{-3}$	Very slight
2	$0.75 \times 10^{-3} \le \Delta/L \le 1.5 \times 10^{-3}$	Slight
3	$1.5 \times 10^{-3} \le \Delta/L \le 3 \times 10^{-3}$	Moderate
4	$3 \times 10^{-3} \le \Delta/L \le 10^{-2}$	Severe
5	$10^{-2} \le \Delta/L$	Very severe

Table A.1: Categories of building damage (Boscardin and Cording (1989))

Appendix 2: Iterative procedure for new analysis tool

Essentially, the procedure uses a non-linear load transfer model of soil behavior (by Kraft et al) with modifications to incorporate cyclic loading capabilities (by Chin and Poulos (1991)) for pile groups (Chow 1986). The procedure is implemented incrementally using incremental loads and displacements (**df, dP, $\mathbf{dP_c}$, du**).

df = vector of incremental load on foundation

dP = vector of incremental soil resistance at each node due to incremental load, **df**

$\mathbf{dP_c}$ = vector of incremental forces at node due to external stiffness (raft, pile, superstructure) due to incremental load, **df**

du = vector of incremental displacement due to incremental load, **df**

$\mathbf{f_{max}}$ = vector of loads (or forces) on foundation for current loading cycle

f = vector of current load on foundation

Solver procedure

[1] ***Initialisation of K_{soil}***

λ_{soil} (and thus $\mathbf{K_{soil}}$) is initialised using equations [28]-[29] and [32] as described in the main text. Initially, **u** = **P** = $\mathbf{P_c}$ = **f** = 0. $\mathbf{K_{pr}}$ and $\mathbf{K_{struct}}$ are also computed.

[2] ***Incremental procedure (for n steps)***

For each step, **f** is incremented by **df** = $\mathbf{f_{max}}$/n. i.e. **f** = **f + df** so that after n steps, the foundations will have been subjected to $\mathbf{f_{max}}$ using an incremental procedure to determine **u** and **P**.

[3] ***Iterative procedure (within each step)***

Loop while Ck < μ (i.e. not converged)

i. Solve for du: $(\mathbf{K_{soil}} + \mathbf{K_{pile}} + \mathbf{K_{raft}} + \mathbf{K_{struct}})\mathbf{du} = \mathbf{df}$
ii. Update displacement: $\mathbf{u_{current}} = \mathbf{du} + \mathbf{u_{previous}}$
iii. Solve for dP_c: $\mathbf{dP_c} = (\mathbf{K_{pr}} + \mathbf{K_{struct}})\mathbf{du}$

iv. Solve for dP: $\mathbf{dP} = \mathbf{df} - \mathbf{dP_c}$

v. Update P: $\mathbf{P_{current}} = \mathbf{dP} + \mathbf{P_{previous}}$

vi. Check that mobilised soil resistance **P** does not exceed ultimate soil resistance $\mathbf{P_f}$**:**

vii. $$\mathrm{P}_{\text{current,i}} = \begin{cases} \mathrm{P}_{\text{current,i}} \text{ if } \mathrm{P}_{\text{current,i}} \leq \mathrm{P}_{\text{f,i}} \\ \mathrm{P}_{\text{f,i}} \text{ if } \mathrm{P}_{\text{current,i}} > \mathrm{P}_{\text{f,i}} \end{cases}$$

viii. Update $\mathbf{K_{soil}}$ and $\boldsymbol{\lambda_{soil}}$ with new values of $\lambda_{soil,ii}$ (where node i is a node on the pile) according to non-linear flexibility coefficients given in [30]-[31] based on β_s and β_b values in [19]-[20] (backbone curve) or [24]-[25] (reloading/unloading curves).

ix. Check for convergence: Ck = Max($\frac{\lambda_{soil,ii,current} - \lambda_{soil,ii,previous}}{\lambda_{soil,ii,current}}$) for all i = node on pile

[4] Once converged, set $\mathbf{u_{previous}} = \mathbf{u_{current}}$ and $\mathbf{P_{previous}} = \mathbf{P_{current}}$. If $\mathbf{f} \neq \mathbf{f_{max}}$, move to step [2] else move to step [5].

[5] If not at final cycle, update $\mathbf{f_{max}}$ with loads from next cyclic loading and update foundation parameters (e.g. new pile parameters, addition of raft etc.) and move to step [2] else move to step [6].

[6] End of procedure.

Note that n, μ can be adjusted. For Bevis Marks simulations, n = 10, μ = 0.001.

New piles added midway through simulation are modeled as normal piles initially with but with zero stiffness ($E_{pile} = 0$). E_{pile} (and thus $\mathbf{K_{pile}}$ and $\mathbf{K_{total}}$) is then readjusted to reflect actual values before the loading cycle it is physically installed (step [5]). Raft thickness is adjusted in a similar way so that $\mathbf{K_{raft}}$ is also adjusted.

Appendix 3: Bevis Marks Pile Loads

Bevis Marks loads can be found from Table A.3. Original building loads are "proven" loads from Soil Consultants Ltd. New building loads = Dead + Live + Wind load from Waterman.

Pile ID	Pile type	Original building Load (kN)	New building Load (kN)
1	Existing	3202	3166
2	Existing	3202	2910
3	Existing	3202	2704
4	Existing	3202	2577
5	Existing	3202	3141
6	Existing	3202	2462
7	Existing	3202	2172
8	Existing	2581	1982
9	Existing	2581	1440
10	Existing	2581	1171
11	Existing	2581	917
12	Existing	2581	2627
13	Existing	1568	1185
14	Existing	1568	1443
15	Existing	1993	1536
16	Existing	1993	1042
17	Existing	1993	430
18	Existing	1993	0.001
19	Existing	1993	1447
20	Existing	4574	2604
21	Existing	2483	3017
22	Existing	2941	2751
23	Existing	2581	2909
24	Existing	2581	2559
25	Existing	1568	2273
26	Existing	1993	2543
27	Existing	1993	2270
28	Existing	1993	2031
29	Existing	1993	2715
30	Existing	4248	2767
31	Existing	4901	5240
32	Existing	4901	5816
33	Existing	4901	6577
34	Existing	8593	5143
35	Existing	1176	1545
36	Existing	8593	4554
37	Existing	4738	3503
38	Existing	4738	5877
39	Existing	4738	4767
40	Existing	4901	5783
41	Existing	4901	6266
42	Existing	4901	6052
43	Existing	4738	3913
44	Existing	4738	5903
45	Existing	4738	4891
46	Existing	4248	4671
47	Existing	4901	4770
48	Existing	4901	5695
49	Existing	4901	5622
50	Existing	8593	6247
51	Existing	1176	1386
52	Existing	8593	3950
53	Existing	4738	3699
54	Existing	4738	5582
55	Existing	4934	3235
56	Existing	1895	621
57	Existing	1895	1317
58	Existing	1895	1043
59	Existing	1895	923
60	Existing	1895	424
61	Existing	1895	452
62	Existing	1895	1095
63	Existing	1895	2048
64	Existing	3137	2275
73	Existing	3202	2650
74	Existing	3202	2315
75	Existing	3202	2219
101	New	0	4110
102	New	0	1349
103	New	0	4782
104.1	New	0	6430
104.2	New	0	6430
105	New	0	4507
106.1	New	0	9110
106.2	New	0	9110
107.1	New	0	7652
107.2	New	0	7652
109	New	0	3777
110	New	0	3070
111.1	New	0	10055
111.2	New	0	10055
112.1	New	0	5941
112.2	New	0	5941
113	New	0	1965
114.1	New	0	8382
114.2	New	0	8382
127	New	0	2779
128	New	0	4447
130	New	0	1990
131	New	0	3017
132	New	0	1590
133	New	0	3353
135	New	0	4594
136	New	0	3319
137	New	0	1524
138	New	0	2173
139.1	New	0	5271
139.2	New	0	5271
140.1	New	0	5385
140.2	New	0	5385
141.1	New	0	5787
141.2	New	0	5787
143	New	0	3729
144	**New**	**0**	**2409**

Table A.3: Bevis Marks pile data

Appendix 4: Evaluation of risk assessment

Original assessment

Prior to the commencement of this research, a risk assessment was conducted to mitigate and prevent potential hazards in this project. Initially, as this research is focused on numerical analysis, the risk assessment focused on hazards associated with computer work, including back injuries, eye strain etc. and listed methods to mitigate these risks such as taking breaks, having a proper posture etc.

Post-project evaluation

The above risks as outlined in the risk assessment were mitigated and no known hazards have occurred.

Fig A.4: Bevis Marks site

However, it is noted that, in the course of this project, a site visit to the Bevis Marks construction site was conducted, which carries additional risks which should have been assessed as part of the risk assessment. As part of the Construction Skills Certification Scheme (CSCS), all personnel at the site were asked to take a health and safety test, which served as a health and safety assessment so that all visiting personnel at the site had a CSCS card. In addition, the contractor provided a 30-min site briefing to warn about the risks. Thus, although the original risk assessment did not take the site visit into account, steps were still taken so that all personnel understood the risks involved and took precaution to mitigate them.